J Neurophysiol 107: 2313–2334, 2012.
First published January 18, 2012; doi:10.1152/jn.00846.2011.

Influence fields: a quantitative framework for representation and analysis of active dendrites

Rahul Kumar Rathour and Rishikesh Narayanan
Molecular Biophysics Unit, Indian Institute of Science, Bangalore, India

Submitted 15 September 2011; accepted in final form 17 January 2012

Rathour RK, Narayanan R. Influence fields: a quantitative framework for representation and analysis of active dendrites. *J Neurophysiol* 107: 2313–2334, 2012. First published January 18, 2012; doi:10.1152/jn.00846.2011.—Neuronal dendrites express numerous voltage-gated ion channels (VGICs), typically with spatial gradients in their densities and properties. Dendritic VGICs, their gradients, and their plasticity endow neurons with information processing capabilities that are higher than those of neurons with passive dendrites. Despite this, frameworks that incorporate dendritic VGICs and their plasticity into neurophysiological and learning theory models have been far and few. Here, we develop a generalized quantitative framework to analyze the extent of influence of a spatially localized VGIC conductance on different physiological properties along the entire stretch of a neuron. Employing this framework, we show that the extent of influence of a VGIC conductance is largely independent of the conductance magnitude but is heavily dependent on the specific physiological property and background conductances. Morphologically, our analyses demonstrate that the influences of different VGIC conductances located on an oblique dendrite are confined within that oblique dendrite, thus providing further credence to the postulate that dendritic branches act as independent computational units. Furthermore, distinguishing between active and passive propagation of signals within a neuron, we demonstrate that the influence of a VGIC conductance is spatially confined only when propagation is active. Finally, we reconstruct functional gradients from VGIC conductance gradients using influence fields and demonstrate that the cumulative contribution of VGIC conductances in adjacent compartments plays a critical role in determining physiological properties at a given location. We suggest that our framework provides a quantitative basis for unraveling the roles of dendritic VGICs and their plasticity in neural coding, learning, and homeostasis.

computational model; voltage-gated ion channels; intrinsic plasticity; learning theory

THE DISCOVERY of voltage-gated ion channels (VGICs) in the dendrites of various neurons, accompanied by findings that VGICs can undergo bidirectional activity-dependent plasticity, constitutes an important breakthrough in neuroscience research. These findings suggest that changes in VGICs and the consequent changes in intrinsic properties, apart from and in conjunction with traditionally considered synaptic changes (Martin et al. 2000; Neves et al. 2008; Stevens 1998), could play important roles in encoding information in a single neuron (Kim and Linden 2007; Mozzachiodi and Byrne 2010; Nelson and Turrigiano 2008; Remy et al. 2010; Sjostrom et al. 2008; Zhang and Linden 2003). Despite this, efforts to incorporate VGICs into learning theory and other physiological frameworks have been far and few (Legenstein and Maass 2011; Stemmler and Koch 1999; Triesch 2007; Weber and Triesch 2008). Furthermore, in most such efforts VGICs are considered as entities that govern only the output end of a neuron, and thus are modeled as modulators of gain/excitability of the neuron. However, especially owing to the presence of VGICs in the dendrites (Johnston and Narayanan 2008; Lai and Jan 2006; Migliore and Shepherd 2002) and their spatially restricted (Frick et al. 2004; Losonczy et al. 2008; Narayanan et al. 2010; Wang et al. 2003) or widespread (Bernard et al. 2004; Narayanan and Johnston 2007, 2008b; Shah et al. 2004) plasticity, it is now recognized that VGICs control various physiological parameters related to the input, integration, and output modules of a neuron (Branco et al. 2010; Branco and Hausser 2011; Hutcheon and Yarom 2000; Llinas 1988; London and Hausser 2005; Magee 2000; Marder et al. 1996; Narayanan and Johnston 2008a; O'Donnell and Nolan 2011; Remme et al. 2010; Sjostrom et al. 2008; Spruston 2008; Stemmler and Koch 1999; Wang 2010). To harness this newly discovered computational power of a single neuron, it is critical that experimentally derived understanding about the diversity and plasticity of dendritic VGICs is incorporated into various models of neuronal physiology.

An important step toward accomplishing this goal is to distinguish the manners in which neuronal function is altered by changes in ligand-gated receptors versus changes in VGICs. A prominent difference between ligand-gated receptors (synapses) and VGICs is that opening of VGICs is not specific to the presynaptic activation of any synapse. Any change in membrane voltage can trigger the opening of a VGIC, and this in conjunction with the connected nature of compartments implies that a VGIC present at a given location alters physiological properties at various adjacent compartments. For instance, the presence or blockade of VGIC conductances at one location influences various physiological measurements at other locations, in a distance-dependent manner (Frick et al. 2003, 2004; Narayanan et al. 2010; Williams 2004). Thus, to understand the roles of dendritic VGICs, it is important to know the influence of a VGIC conductance located at a neuronal compartment toward altering various physiological parameters of other compartments within the same neuron.

In this study, we define and analyze the "influence field" as a quantitative abstraction of the influence of a spatially confined cluster of VGICs on a physiological parameter. We develop this abstraction to quantitatively analyze interactions of VGICs in different neuronal compartments, accounting for the specific locations of VGICs and the connected nature of these compartments. Employing this framework, we quantitatively demonstrate that the extent of influence of a VGIC conductance is largely independent of the conductance magni-

Address for reprint requests and other correspondence: R. Narayanan, Molecular Biophysics Unit, Indian Institute of Science, Bangalore 560 012, India (e-mail: rishi@mbu.iisc.ernet.in).

tude but is heavily dependent on the specific physiological property and background conductances. Through our analyses employing a range of measurements, we demonstrate that the influences of different VGIC conductances located on a thin dendritic branch are confined within that dendritic branch. This would imply that VGICs located in thin dendritic branches do not influence computations outside that dendritic branch, thus constituting an additional mechanism by which small dendritic branches can compartmentalize computations (Branco and Hausser 2010; Govindarajan et al. 2010; Larkum et al. 2009; London and Hausser 2005; Losonczy and Magee 2006; Losonczy et al. 2008; Nevian et al. 2007; Poirazi et al. 2003; Polsky et al. 2004). Next, we demonstrate that the extent of influence of a VGIC that alters action potential propagation is localized only if actively sustained. If propagation ceases to be active, the extent of influence becomes spatially widespread, thus constituting an important constraint for the influence of localized plasticity in dendritic VGICs (Frick et al. 2004). Finally, using influence fields to estimate functional properties from gradients in dendritic VGIC conductances, we demonstrate that the cumulative contribution of VGIC conductances in adjacent compartments plays a critical role in determining physiological properties at a given location. We propose that our framework offers a crucial quantitative link between dendritic VGICs and their ability to alter neural coding, metaplasticity, homeostasis, and network dynamics.

MODELS AND METHODS

We employed two distinct models for the analyses presented in this study. The first was a simple model that consists only of two cylinders (referred to as the ball-and-stick model here), and the other was a morphologically realistic model built from three-dimensional (3D) reconstructions of hippocampal CA1 pyramidal neurons.

Ball-and-stick model. The ball-and-stick model consisted of two cylinders, with one representing the somatic section (50-μm diameter, 50-μm length) and the other forming the dendritic section (500-μm length, 2-μm diameter) (Fig. 1*A*). The dendritic section was further subdivided into 100 compartments for accommodating isopotential-

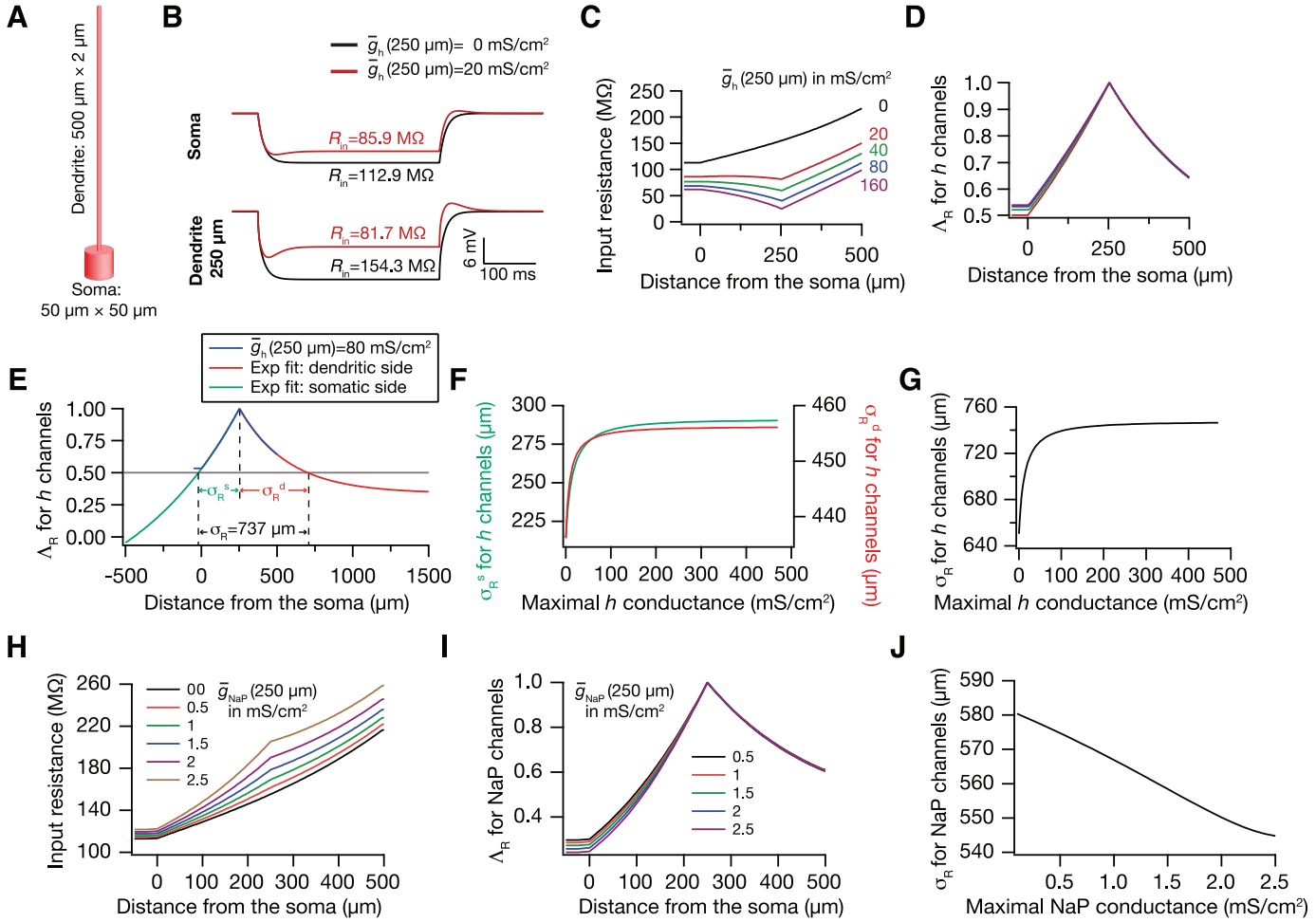

Fig. 1. Local presence of an *h*-channel cluster exerts widespread influence on input resistance measurement. *A*: schematic of the 2-cylinder piston model used to establish the basic quantitative framework for analyzing the influence fields. *B*: voltage traces in response (somatic, *top*; 250 μm dendritic, *bottom*) to a local injection of a hyperpolarizing current pulse (100 pA for 350 ms) in the absence (black) and the presence (red) of an h-channel cluster located at a dendritic location 250 μm from the soma. *C*: input resistance (R_{in}) measured along the somatodendritic axis in the absence (black) and presence of an h-channel cluster, located at 250 μm from the soma and of varying conductance densities ($\bar{g}_h$) (colors). *D*: normalized influence of an h-channel cluster on R_{in} (Λ_R) for various values of $\bar{g}_h$, computed from the plots in *C*. Color codes are the same as those in *C*. *E*: illustration of the quantitative estimation of the extent of influence fields using exponential functions (see MODELS AND METHODS). *F*: effect of $\bar{g}_h$ on the extent of influence of an h-channel cluster on R_{in} (σ_R), along the somatic (green) and dendritic (red) flanks. *G*: σ_R as a function of $\bar{g}_h$ suggests a small and saturating increase in the extent of the influence of h channels on R_{in} as a function of $\bar{g}_h$. *H–J*: similar to *C*, *D*, and *G*, but analysis of Λ_R involves persistent Na^+ conductance ($\bar{g}_{NaP}$).

like constraints on individual compartments. The passive electrical parameters were uniform across the somatic and dendritic compartments and were set as follows: specific membrane resistivity $R_m = 12$ kΩ·cm^2, specific membrane capacitance $C_m = 1$ μF/cm^2, axial resistivity $R_a = 100$ Ω·cm.

Morphologically realistic model. A reconstructed hippocampal CA1 pyramidal neuron (*n123*) obtained from NeuroMorpho.Org (Ascoli et al. 2007), originally reconstructed by Pyapali et al. (1998), was used as the substrate for all morphologically realistic simulations. Passive electrical parameters were set such that the local input resistance (R_{in}, defined below) remained almost constant (~120 MΩ) throughout the trunk (Narayanan and Johnston 2007). The specific membrane capacitance C_m was set at 1 μF/cm^2. Specific membrane resistance R_m and intracellular resistivity R_a for various compartments along the somato-apical trunk as functions of radial distance of the compartment from the soma, x, were set according to the following equations (Narayanan and Johnston 2007; Poirazi et al. 2003):

$$R_m(x) = \frac{R_m^{som} + \left(R_m^{end} - R_m^{som}\right)}{1 + \exp\left(\frac{300 - x}{50}\right)} \text{ k}\Omega.\text{cm}^2 \quad (1)$$

$$R_a(x) = \frac{R_a^{som} + \left(R_a^{end} - R_a^{som}\right)}{1 + \exp\left(\frac{210 - x}{50}\right)} \ \Omega.\text{cm} \quad (2)$$

where $R_m^{som} = 65$ kΩ·cm^2 and $R_a^{som} = 50$ Ω·cm were values at the soma and $R_m^{end} = 35$ kΩ·cm^2 and $R_a^{end} = 30$ Ω·cm were values assigned to the terminal end of the apical trunk (which was ~425 μm distant from the soma for the reconstruction under consideration). The basal dendrites and the axonal compartments had somatic R_m and R_a, and apical obliques had the same R_m and R_a as the trunk compartment from which they originated. This neuronal model was compartmentalized by using the d_λ rule (Carnevale and Hines 2006) to ensure that each compartment is smaller than 0.1 λ_{100}, where λ_{100} is the space constant, computed at 100 Hz, of the section under consideration.

Channel kinetics and distribution. Our study includes six different types of biophysically realistic VGIC models: Na^+, A-type (K_A), M-type (K_M), and delayed-rectifier (K_{DR}) K^+ channels, persistent Na^+ conductance (NaP), and hyperpolarization-activated h channels. The kinetic schemes for Na^+, K_{DR}, and K_A channels were adopted from Migliore et al. (1999), and the h channel was modeled as in Poolos et al. (2002). Persistent Na^+ channel kinetics were taken from Uebachs et al. (2010). The kinetics for the M channel were adopted from Shah et al. (2008), with the half-maximal activation voltage changed to -10 mV, to account for experimental results from cell-attached recordings of these channels in CA1 pyramidal neurons (Chen and Johnston 2004). Reversal potentials for Na^+, K^+, and h channels were set at 55, -90, and -30 mV, respectively.

While assessing properties associated with action potential propagation in the ball-and-stick model, Na^+ and K_{DR} conductances were distributed equally in soma and dendrite: $\bar{g}_{Na} = 40$ mS/cm^2 and $\bar{g}_{KDR} = 10$ mS/cm^2. In the multicompartmental model, maximal conductance values of Na^+ ($\bar{g}_{Na} = 45$ mS/cm^2) and K_{DR} ($\bar{g}_{KDR} = 15$ mS/cm^2) channels in different compartments were set such that the action potential amplitude was ~110 mV across all compartments when the A-type K^+ conductance was absent (Hoffman et al. 1997; Migliore et al. 1999). $\bar{g}_{Na}$ in the axon initial segment was set fivefold higher compared with its somatic value (Fleidervish et al. 2010). The rest of the axon was treated as passive. To account for slow inactivation of dendritic Na^+ channels (Colbert et al. 1997), an additional inactivation gate variable was included (Migliore et al. 1999).

A-type K^+ conductance was set as a linearly increasing gradient as a function of radial distance from the soma, x, and was adjusted such that the backpropagating action potential (bAP) amplitude was ~8–10 mV at the terminal end of the apical trunk (Hoffman et al. 1997; Migliore et al. 1999):

$$\bar{g}_{KA}(x) = 22\left(1 + \frac{5x}{100}\right) \text{mS/cm}^2 \quad (3)$$

To accommodate experimental observations on differences between the activation parameters of the A-type K^+ channel in CA1 pyramidal cells (Hoffman et al. 1997), two different models for the A-type K^+ conductance were used as in Migliore et al. (1999) and were spatially segregated. Specifically, the proximal version was used for compartments with radial distances <100 μm from the soma, beyond which point the distal A-type K^+ conductance model was used.

In simulations that involved gradients in h-channel properties, the maximal conductance value for the h conductance for compartments along the somatodendritic trunk, as a function of radial distance from the soma, x, was set as a sigmoidal function:

$$\bar{g}_h(x) = 25\left(1 + \frac{95}{1 + \exp\left(\frac{350 - x}{5}\right)}\right) \mu\text{S/cm}^2 \quad (4)$$

The basal dendrites had somatic $\bar{g}_h$, and apical obliques had the same $\bar{g}_h$ as the trunk compartment from which they originated (Narayanan and Johnston 2007). Along the somato-apical trunk, the half-maximal activation voltage for h channels was -82 mV for $x \leq 100$ μm, linearly varied from -82 mV to -90 mV for 100 μm $\leq x \leq 300$ μm, and was -90 mV for $x > 300$ μm (Magee 1998). The specific values associated with the sigmoidal function above were set such that at -65 mV R_{in} reduced from ~65 MΩ to 25 MΩ along the axis of the somatodendritic trunk, accompanied by a corresponding increase in resonance frequency (f_R) from 3 to 12 Hz (Narayanan and Johnston 2007).

Measurements. R_{in} of a compartment was measured from the steady-state voltage response of the compartment to a 100-pA hyperpolarizing current pulse (for 300 ms) and was computed as the ratio between the steady-state voltage response and the injected current amplitude. f_R was calculated along the dendrite by giving a chirp stimulus: a sinusoidal current wave with constant amplitude (50 pA) with frequency linearly increasing from 0 to 25 Hz in 25 s. The Fourier transform of voltage response of the chirp stimulus was divided by the Fourier transform of the chirp stimulus to generate the impedance amplitude profile. The frequency at which the impedance amplitude reached its maximum was taken as f_R (Hutcheon and Yarom 2000; Narayanan and Johnston 2007). Action potentials were generated by injecting a 1-nA depolarizing current for 2 ms in the soma, and the amplitude of the action potential was measured as the difference between its peak and the resting membrane potential. These measurements were chosen for this study in order to span subthreshold and suprathreshold, propagating and nonpropagating measurements that are sensitive to changes in VGICs that are predominantly present in hippocampal CA1 pyramidal neuron dendrites (Johnston and Narayanan 2008; Lai and Jan 2006; Migliore and Shepherd 2002).

Computational details. All simulations were performed with the NEURON simulation environment (Carnevale and Hines 2006). Unless otherwise stated, simulations were performed with resting membrane potential set at -65 mV. Temperature was set at 34°C, and ion channel kinetics were adjusted appropriately, accounting for their experimentally determined Q_{10} factors. Simulations involving the M-type K^+ current were performed at -35 mV, owing to the depolarized activation range of the M current. The default integration time step was set at 25 μs. Computation of f_R and other measurements (above), numerical quantification of influence fields using curve fitting algorithms, and analyses of influence fields pertaining to linearity and parametric dependencies (see RESULTS) were performed with custom-built software written within the IGOR Pro (Wavemetrics) programming environment.

Quantifying influence fields. The influence field of a given ion channel cluster located at x_i on a physiological measurement, M, is

quantified through the normalized influence factor, $\Lambda_M(x; x_i)$, defined as follows:

$$\Lambda_M(x; x_i) = \frac{\mathrm{IF}_M(x; x_i)}{\max_x \mathrm{IF}_M(x; x_i)} \quad (5)$$

where x spans various locations along a neuronal axis, and IF(x) depicts the unnormalized influence factor, defined as:

$$\mathrm{IF}_M(x; x_i) = \frac{|M_{\mathrm{org}}(x) - M_{\mathrm{new}}(x)|}{M_{\mathrm{org}}(x)} \quad (6)$$

where M_{org} is the initial measurement obtained in the absence of the ion channel cluster at location x_i and M_{new} is the measurement obtained after insertion of the ion channel cluster at location x_i. As an example, R_{in} is measured at various locations along the neuron in the absence of any active conductance [thus providing us with $M_{\mathrm{org}}(x)$ in the above equation; see Fig. 1, *B* and *C*]. Next, an h-channel cluster (an h conductance of a given density) was inserted at a dendritic location 250 μm away from the soma, and measurements of R_{in} were obtained again at all locations along the neuron [providing us with $M_{\mathrm{new}}(x)$; see Fig. 1, *B* and *C*]. Plugging these values into *Eq. 6* yielded $\mathrm{IF}_R(x;250\ \mu\mathrm{m})$, the unnormalized influence factor of an h-channel cluster dendritically located at (x_i=) 250 μm away from the soma, on R_{in}. Normalizing $\mathrm{IF}_R(x;250\ \mu\mathrm{m})$ with *Eq. 5* would then yield $\Lambda_R(x; 250\ \mu\mathrm{m})$, with R representing resistance and $x_i = 250\ \mu$m (the similarity of the shape of Λ to the functional form of a typical influence field was a reason for the choice of Λ as the notation for normalized influence factor; Fig. 1*D*). In this case, the influence of the ion channel cluster on the measurement would be maximal at x_i, thus making

$$\max_x \mathrm{IF}_R(x; x_i) = \mathrm{IF}_R(x_i; x_i)$$

thus always making $\Lambda_R(x_i; x_i) = 1$.

To quantitatively understand the influence field, we assigned a functional form for it. Owing to the sharp transition of $\Lambda_M(x; x_i)$ (Fig. 1*D*) at x_i, we characterize it using two exponentials, one spanning the somatic flank of Λ_M (from the soma to x_i) and another spanning its dendritic flank (from x_i to the end of the dendritic compartment). Specifically, $\Lambda_M(x; x_i)$ is fit with two exponentials as follows:

$$\Lambda_M(x; x_i) = \begin{cases} A_M^{\mathrm{s}} + B_M^{\mathrm{s}} \exp\left[(x - x_M^{\mathrm{s}})/\tau_M^{\mathrm{s}}\right] & : \quad 0 \le x \le x_i \\ A_M^{\mathrm{d}} + B_M^{\mathrm{d}} \exp\left[-(x - x_M^{\mathrm{d}})/\tau_M^{\mathrm{d}}\right] & : \quad x_i \le x \le \mathrm{L_d} \end{cases} \quad (7)$$

where L_{d} is the total length of the dendritic compartment. τ_M^s and τ_M^d, respectively, represent the decay of $\Lambda_M(x; x_i)$ along its somatic and dendritic flanks (Fig. 1*E*). With this formulation, we extracted metrics of $\Lambda_M(x; x_i)$ that would help in quantitatively understanding the extent of influence of an ion channel cluster located at x_i on measurement M. We define the extent of the influence field, $\sigma_M(x; x_i)$, as the full width at half-maximum (FWHM) of $\Lambda_M(x; x_i)$. Figure 1*E* illustrates the process of obtaining a functional form of $\Lambda_M(x; x_i)$ with two exponentials and computing the extent of the influence field, $\sigma_M(x; x_i)$, as the sum of the half-maximal widths along the somatic and dendritic flanks. Specifically, we compute $\sigma_M(x; x_i)$ as the sum of half-maximal widths along the somatic and dendritic flanks of $\Lambda_M(x; x_i)$, using the functional form obtained in *Eq. 7* as follows:

$$\sigma_M(x; x_i) = \sigma_M^{\mathrm{s}}(x; x_i) + \sigma_M^{\mathrm{d}}(x; x_i) \quad (8)$$

where $\sigma_M^s(x; x_i)$ is the half-maximal width along the somatic flank, computed as:

$$\sigma_M^{\mathrm{s}}(x; x_i) = \left| x_i - x_M^{\mathrm{s}} + \tau_M^{\mathrm{s}} \ln\left(\frac{0.5 - A_M^{\mathrm{s}}}{B_M^{\mathrm{s}}}\right)\right| \quad (9)$$

and $\sigma_M^d(x; x_i)$ is the half-maximal width along the dendritic flank, computed as:

$$\sigma_M^{\mathrm{d}}(x; x_i) = \left| x_i - x_M^{\mathrm{d}} + \tau_M^{\mathrm{d}} \ln\left(\frac{0.5 - A_M^{\mathrm{d}}}{B_M^{\mathrm{d}}}\right)\right| \quad (10)$$

The FWHM was used as the default; in cases where the exponential fit never reached a value of 0.5, we computed the extent as full width at three-quarter maximum (FWTQM).

Quantification of summation of influence fields. To assess how influence fields of different ion channel clusters interact, we calculated their combined influence field, as follows:

$$\Lambda_R(x; x_1, x_2) = \frac{\mathrm{IF}_R(x; x_1, x_2)}{\max_x \mathrm{IF}_R(x; x_1, x_2)} \quad (11)$$

Then we calculated the influences of the presence of either of these two clusters individually, computed the linear sum of the two influence fields, and normalized this linear sum to compute the normalized linearly summed influence field as follows:

$$NLS_R(x; x_1, x_2) = \frac{\mathrm{LS}_R(x; x_1, x_2)}{\max_x \mathrm{LS}_R(x; x_1, x_2)} \quad (12)$$

where LS_R is the linear sum of the influence fields of two ion channel clusters located at x_1 and x_2 along the dendrite and was calculated as:

$$\mathrm{LS}_R(x; x_1, x_2) = \mathrm{IF}_R(x; x_1) + \mathrm{IF}_R(x; x_2) \quad (13)$$

where $\mathrm{IF}_R(x; x_1)$ and $\mathrm{IF}_R(x; x_2)$ represent influence fields of ion channel cluster located at x_1 and x_2 positions (computed as in *Eq. 6*). Finally, we quantified the linearity of summation of influence fields as the ratio between the area under the combined influence field (*Eq. 11*) and that under the normalized linearly summed influence field (*Eq. 12*) and defined it as the linearity index (LI) for influence fields:

$$\mathrm{LI}(x_1, x_2) = \frac{\int_0^{L_{\mathrm{d}}} \Lambda_R(x; x_1, x_2)\mathrm{d}x}{\int_0^{L_{\mathrm{d}}} \mathrm{NLS}_R(x; x_1, x_2)\mathrm{d}x} \quad (14)$$

By this definition, LI would be 1 if the summation is linear and would be greater or lesser than unity when the summation is supralinear or sublinear, respectively.

RESULTS

Neuronal dendrites express numerous VGICs, typically with spatial gradients in their densities and properties (Johnston and Narayanan 2008; Lai and Jan 2006; Migliore and Shepherd 2002). Recent literature has demonstrated that VGICs can undergo plasticity in response to learning and in conjunction with in vitro activity-dependent protocols that are typically thought to be involved in inducing synaptic plasticity (Kim and Linden 2007; Mozzachiodi and Byrne 2010; Nelson and Turrigiano 2008; Remy et al. 2010; Sjostrom et al. 2008; Turrigiano 2011; Zhang and Linden 2003). To understand dendritic VGICs, their gradients, and their plasticity and to incorporate them into various learning theory models, it is critical to incorporate the connected nature of neuronal compartments. Owing to this connectedness, the presence of VGIC conductances at one location can alter physiological properties at other locations within the neuron. An example of such spatially widespread influence of a localized VGIC conductance is depicted in Fig. 1. Here, we had inserted a single h-channel conductance cluster ($\bar{g}_{\mathrm{h}} = 80$ mS/cm^2) at a dendritic location 250 μm away from the soma in an otherwise passive ball-and-stick model. Insertion of an h conductance into a dendritic

compartment would expectedly reduce the local input resistance (R_{in}) at that compartment (from 154.3 MΩ to 81.7 MΩ; Fig. 1*B*). In addition, because of the connected nature of the various compartments, R_{in} at other locations also underwent significant reductions, although the ion channel cluster was present only at one location. For instance, R_{in} at the somatic compartment was reduced from 112.9 MΩ to 85.9 MΩ (Fig. 1*B*), even though no additional conductance was added to any other compartment other than the one at 250 μm on the dendrite.

To quantify this spread of influence of the VGIC on the measurement, we plotted R_{in} as a function of distance in the absence of any active components (Fig. 1*C*) and in the presence of a single h-channel cluster (at 250 μm) of various conductance values (Fig. 1*C*). We computed the reductions in R_{in} at all locations due to the presence of the single h-channel cluster at 250 μm (differences between black and colored traces in Fig. 1*C*) and normalized these reductions with respect to the reduction at the cluster location. We found that the reduction of R_{in} was maximal at the location of the cluster and reduced with increase in distance from the cluster (Fig. 1*D*). We called this plot the "influence field" of the h-channel cluster on R_{in}, as it quantifies the distance-dependent impact of the cluster on R_{in}. To understand the spatial spread of the influence of a given VGIC cluster, we also computed the full width at half-maximum (FWHM) of this normalized plot and called it the extent of the influence field (see MODELS AND METHODS for more details).

In the sections that follow, we analyze the influence field as a quantitative abstraction of the distribution, in neuronal space, of the influence of a spatially confined cluster of VGICs on various physiological measurements. The nature and extent of such influence fields would alter the manner in which different VGICs in different compartments interact with each other and the manner in which incoming synaptic inputs are processed. We propose this as a first step toward the incorporation of VGICs, their numerous physiological roles, and their activity-dependent plasticity into learning frameworks and other models of cellular neurophysiology.

Influence fields of VGICs were coupled to measurements. Are influences of a given VGIC cluster different for different measurements? To address this, we compared influence fields (see MODELS AND METHODS) of the same h-channel cluster, located at 250 μm from the soma, on two physiologically relevant measurements, input resistance (R_{in}) and resonance frequency (f_R), in the ball-and-stick model. We noted that the extent of influence along the dendritic flank was greater than that along the somatic flank for both R_{in} (Fig. 1*D*) and f_R (not shown). Such asymmetry should be expected given the presence of the large somatic compartment on one end of the dendrite.

Next, we assessed the role of h-channel conductance in shaping the extent of influence fields for both R_{in} and f_R. We found a very small and saturating increase in extent of influence for R_{in} (σ_R) as a function of $\bar{g}_h$, suggesting that the influence field was largely invariant to the maximal h-channel conductance in this case (Fig. 1, *F* and *G*). In contrast, the extent of influence for f_R (σ_f) decreased as a function of increase in $\bar{g}_h$ (not shown). We also performed a detailed sensitivity analysis with respect to the entire set of passive and h-channel parameters associated with the model (Table 1) and found contrasting differences between R_{in} and f_R in terms of the sensitivities of their influence fields to various parameters. As the same h-channel cluster was employed for measuring influence fields of R_{in} and f_R, this suggested that influence fields were different for different physiological measurements even if the measurements were made in the presence of the same VGIC cluster.

If influence fields were coupled to measurements, then influence field properties and their parametric sensitivities corresponding to a measurement should be the same even if that measurement were to be altered by another VGIC. To test this postulate, we chose the M-type K^+ channel, another resonating conductance that regulates both R_{in} and f_R (Hu et al. 2002). Using M-type K^+ conductance, we repeated all the

Table 1. *Sensitivity analysis for extent of influence fields corresponding to* R_{in} and f_R in ball-and-stick model

Effects of Increase in	Range Tested	Extent of IF of R_{in}, σ_R			Extent of IF of f_R, σ_f	
		Localized Presence of			Localized Presence of	
		g_h	g_M	g_{NaP}	g_h	g_M
R_m	1–25 kΩ·cm^2	Increases	Increases	Increases	Increases	Increases
R_a	50–300 Ω·cm	Decreases	Decreases	Decreases	Decreases	Decreases
C_m	1–4 μF/cm^2	No effect	No effect	No effect	Decreases	Decreases
Dendritic diameter	1–5 μm	Increases	Increases	Increases	Increases	Increases
V_m	−180 to −30 mV	Decreases	Decreases	Decreases	Increases	Decreases
$\bar{g}_h$	0–500 mS/cm^2	Increases*			Decreases	
$\bar{g}_M$	0–300 mS/cm^2		Decreases*			Decreases
$\bar{g}_{NaP}$	0–2.5 mS/cm^2			Decreases*		
$V_{1/2}$	−180 to −20 mV	Increases	Increases	Increases	Decreases	Increases
Activation time constant	5–500 ms	No effect	No effect	No effect	Increases	Increases
Distance of cluster from soma	0–500 μm	Increases	Increases	Increases	Increases	Increases

Sensitivity analysis for the extent of influence fields (IFs) corresponding to input resistance (R_{in}) and resonance frequency (f_R) in the ball-and-stick model. The parameters on which the analysis was performed form the first column, and the second column indicates the tested range of the corresponding parameter. Other columns correspond to changes observed in σ_R and σ_f for increases in the parameters given in the first column corresponding to type of ion channel (top row: *columns 3–7*). Data presented here as well as in Table 2 were derived after plotting the extent of IFs as functions of the each of the mentioned parameters varied over the range specified in the table (e.g., Fig. 1*G* for dependence of Λ_R on $\bar{g}_h$). *Very small changes. All σ_f values calculated at 0.95 Λ_f. Increase in $V_{1/2}$ and V_m refers to depolarizing shift in the respective voltages. $V_{1/2}$ and activation time constant refer to the corresponding parameters with respect to either the h or the M channel. R_m, membrane resistivity; R_a, axial resistivity; C_m, membrane capacitance.

experiments that we had performed with h channels (Fig. 1 and Table 1) and compared these results with those obtained with the h-channel clusters (Table 1). On the basis of these analyses, we found that influence fields and their parametric dependencies corresponding to either R_{in} or f_R were largely similar (Table 1), irrespective of whether h or M-type channels were used to alter their values. However, specific channel properties did alter parametric dependencies in some cases, especially in parameters related to membrane voltage. As the h current is a hyperpolarization-activated inward current and the M current is a depolarization-activated outward current, dependencies of σ_f and σ_R on membrane voltage were exactly opposite to each other for the h and M currents (Table 1). Similar dichotomies were observed with changes in activation $V_{1/2}$ and maximal conductance value of either the M or the h channels (Table 1).

So far we have analyzed influence field properties for input resistance (R_{in}) corresponding to restorative conductances i.e., the h- and M-type K^+ channels. Next, we asked whether properties of influence field for input resistance (Λ_R) held true for regenerative conductances that enhance membrane excitability. The postulate was that if influence fields were largely coupled to specific physiological measurements rather than to specific VGICs, then properties of influence fields should be the same even if physiological measurements were altered by using a regenerative conductance. To test this, we used persistent Na^+ conductance, a regenerative conductance that increases R_{in} (Vervaeke et al. 2006). Similar to h channel and M-type K^+ channel, where local presence of these conductances decreased R_{in} along the entire trunk (Fig. 1*C*), we found that local presence of persistent Na^+ conductance (g_{NaP}) increased R_{in} along the entire somato-apical trunk (Fig. 1*H*), yielding an influence field very similar to those of restorative conductances (Fig. 1*I*). As observed previously with h and M-type K^+ conductances, we found that the shape of the influence field was asymmetric and the extent of influence was higher toward the dendritic flank compared to the somatic flank (Fig. 1*I*). We also found a small decrease in extent of influence for R_{in} (σ_R) as a function of the maximal persistent Na^+ conductance, $\bar{g}_{NaP}$ (Fig. 1*J*). Finally, we performed detailed sensitivity analysis to study the properties of influence field for input resistance (Λ_R) corresponding to g_{NaP} and found that the properties of Λ_R were very similar to those observed with h and M-type K^+ conductances (Table 1). Together, these results suggested that influence fields were largely coupled to specific physiological measurements, rather than to specific VGICs.

Parametric dependencies of influence fields and conductance attenuation are related. So far our analysis of Λ_R and Λ_f using the h channel, the M-type K^+ channel, and the persistent Na^+ channel has revealed certain unique properties of these influence fields. Specifically, we observed that the magnitude of conductance had minimal effect on the extent of influence fields. On the other hand, we found that passive electrical parameters and location of the channel cluster were major determinants of the extent of influence fields. What aspect of neuronal physiology contributes to such differential dependence of influence field extents on these different parameters? As influence fields form a quantification mechanism for the distance dependence of a conductance at a given location, we postulated that the differential sensitivity of conductance attenuation along the dendritic arbor (Williams 2004) to these different parameters could be the basis for such variability. Under such a postulate, and given our results on influence fields above, conductance attenuation should largely be invariant to the conductance magnitude of the cluster used to compute influence fields. Furthermore, the parameter that increases the extent of influence fields (for example, R_m) will reduce the conductance attenuation, and that which decreases the extent of influence fields (for example, R_a) would enhance the conductance attenuation.

To test this postulate and thereby understand the properties of influence fields, we quantified conductance attenuation as the relative reduction of R_{in} produced by identical conductance changes delivered at the recording site and a remote site (Williams 2004). Specifically, if ΔR_{in}^{rec} and ΔR_{in}^{rem} were the measured R_{in} changes when the conductance changes were delivered at the recording site and a remote site, respectively, then conductance attenuation, A_g, was computed as:

$$A_g = \frac{\Delta R_{in}^{rec} - \Delta R_{in}^{rem}}{\Delta R_{in}^{rec}} \quad (15)$$

To test our postulate on the relationships between A_g and influence fields, we computed A_g with the recording site fixed at a dendritic location 250 μm away from the soma and with varying remote locations (Fig. 2, *A–C*). To test whether A_g was invariant to the amounts of conductance changes, we computed A_g for various values of h conductances inserted at the recording or different remote locations (Fig. 2*D*). We found that, with respect to a given remote location, A_g was largely independent of conductance magnitude (Fig. 2*D*). However, as the remote location was varied, the magnitude of A_g was different (Fig. 2*D*), which should be expected because conductance attenuation depends on the distance between the remote and recording locations (Williams 2004). Thus conductance invariance of A_g translates to conductance invariance of influence fields, and the dependence of A_g on location translates to location dependence of influence fields as well (Table 1). Furthermore, we also noted that the asymmetry in influence fields (Fig. 1, *D–G*) was reflected as an asymmetry between A_g computed at equidistant (with reference to the recording location, 250 μm; Fig. 2*D*) points close to (100 μm location) and away from (400 μm location) the soma. From these results, we reasoned that the dependencies of influence fields for R_{in} on different parameters had their bases in the dependence of A_g on those specific parameters.

To further validate this conclusion, we performed similar analysis with a regenerative conductance g_{NaP} and arrived at similar results (Fig. 2*E*). Furthermore, when we performed similar analyses with fixed h conductance, while varying specific membrane resistivity (R_m) or axial resistivity (R_a) (Fig. 2, *F* and *G*), we found that A_g was no longer constant when these parameters varied across the dendrite. Specifically, A_g decreased with increase in R_m (Fig. 2*F*) while it increased with increase in R_a (Fig. 2*G*), which is to be expected given the dependence of conductance attenuation on these cable properties. These results suggested that an increase in R_m would increase the influence field for R_{in} and an increase in R_a would decrease the influence field for R_{in}, which was consistent with our results on influence fields (Table 1). From these results, we concluded that the dependence of influence fields on various parameters was directly related to dependence of conductance attenuation on those parameters, and

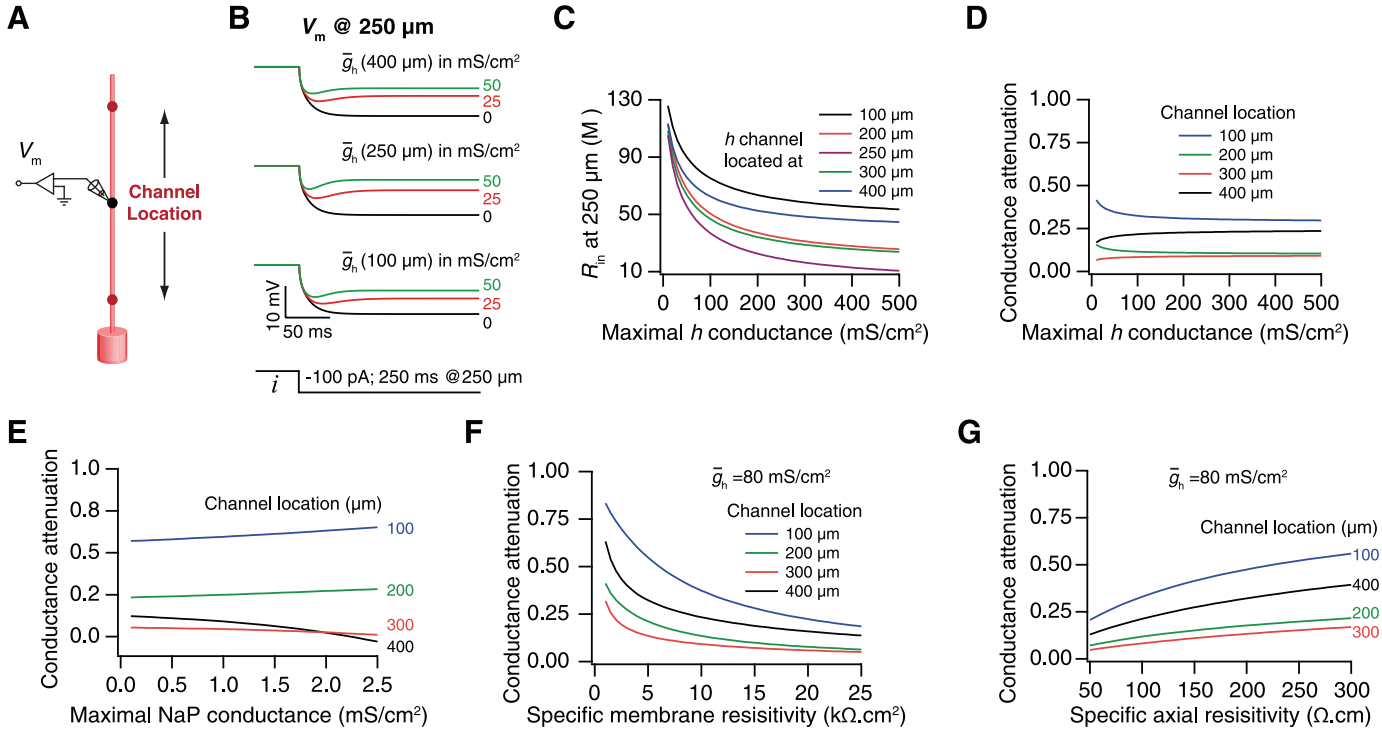

Fig. 2. Conductance attenuation between 2 locations is largely independent of conductance magnitude. *A*: schematic of experimental design showing channel cluster locations and recording site. *B*: voltage traces recorded at the dendritic location 250 μm from the soma in response to a hyperpolarizing current pulse for various values of h conductance inserted at different locations along the dendrite. The dendritic location where the conductance was inserted is provided within parentheses, and the traces and corresponding h conductance values are color-coded. *C*: R_{in} computed at the dendritic location 250 μm from the soma for various values of h conductance inserted at different locations along the dendrite. These values were employed to compute conductance attenuation as in *Eq. 15*. *D*: conductance attenuation computed for various values of h conductance inserted at different locations along the dendrite. Note that for a given location of h conductance, conductance attenuation is largely independent of conductance magnitude. *E*: similar to *D*, but computation of conductance attenuation was done using persistent Na^+ conductance. *F*: conductance attenuation computed for various values of specific membrane resistance (R_m) with fixed magnitude of h conductance inserted at different locations along the dendrite. *G*: conductance attenuation computed for various values of specific axial resistance (R_a) with fixed magnitude of h conductance inserted at various locations along the dendrite. All voltage recordings were performed at the dendritic location 250 μm away from the soma for all panels.

that such a relationship provides an explanation for why a differential dependence of influence fields on different parameters was observed. However, caution should be exercised in extending this analysis to measurements based on time-varying signals, as A_g constitutes a steady-state frequency-independent measurement. In such cases, it would be appropriate to employ a frequency-dependent admittance attenuation measurement, which could be derived from input impedance instead of R_{in} in *Eq. 15*. Finally, it should be noted that both influence fields and conductance attenuation are normalized measures, and invariance of these quantities to a certain parameter does not mean that the underlying physiological measurement is invariant to the parameter. For instance, although Λ_R and A_g were invariant to h-channel conductance, R_{in} was different for different $\bar{g}_h$ (Fig. 1*C*).

Active dendrites reduced the extent of influence fields in morphologically realistic neuronal models. We next turned to analyzing influence fields in a morphologically realistic neuronal model. To do this, we employed a reconstructed hippocampal CA1 pyramidal neuron and set its passive electrical parameters based on previous experimental observations (see MODELS AND METHODS). We employed two different models, one made of only the passive dendritic tree (called the passive 3D model) and the other having an experimentally constrained h-channel gradient across the dendritic arbor (see MODELS AND METHODS) (called the active 3D model). As in the ball-and-stick model, we placed an h-channel cluster of varying conductances at the middle of the apical trunk (457 μm from the soma; path distance) and measured R_{in} along the somato-apical trunk before and after the placement of the cluster in both passive as well as active 3D models. Consistent with our observation in the ball-and-stick model (Fig. 1*C*), R_{in} decreased not only at the location where the cluster was present but also throughout the trunk in passive (Fig. 3*A*) and active (Fig. 3*F*) models. Furthermore, the extent of influence of the cluster on R_{in} was largely independent of the conductance magnitude in the passive (Fig. 3, *B* and *C*) as well as active (Fig. 3, *G* and *H*) 3D models.

Apart from these similarities in the two 3D models, we also noted a number of differences in their influence field properties. The extent of the influence field was much lower in the active dendrite (σ_R was ~130 μm; Fig. 3*H*) compared with the passive neuronal model (σ_R was ~420 μm; Fig. 3*C*) because of the presence of high background conductance (cf. case where R_m was decreased in the ball-and-stick model; Table 1). Furthermore, in contrast to the ball-and-stick and the passive 3D model, where asymmetry of influence field favored its extent along the dendritic flank ($\sigma_R^d > \sigma_R^s$) (Fig. 1, *D* and *E*, Fig. 3*B*), in the active 3D model, asymmetry in the influence field was reversed and favored its extent along the somatic flank ($\sigma_R^d < \sigma_R^s$) (Fig. 3*G*). We reasoned that the extent along the dendritic flank was lower because the background conduc-

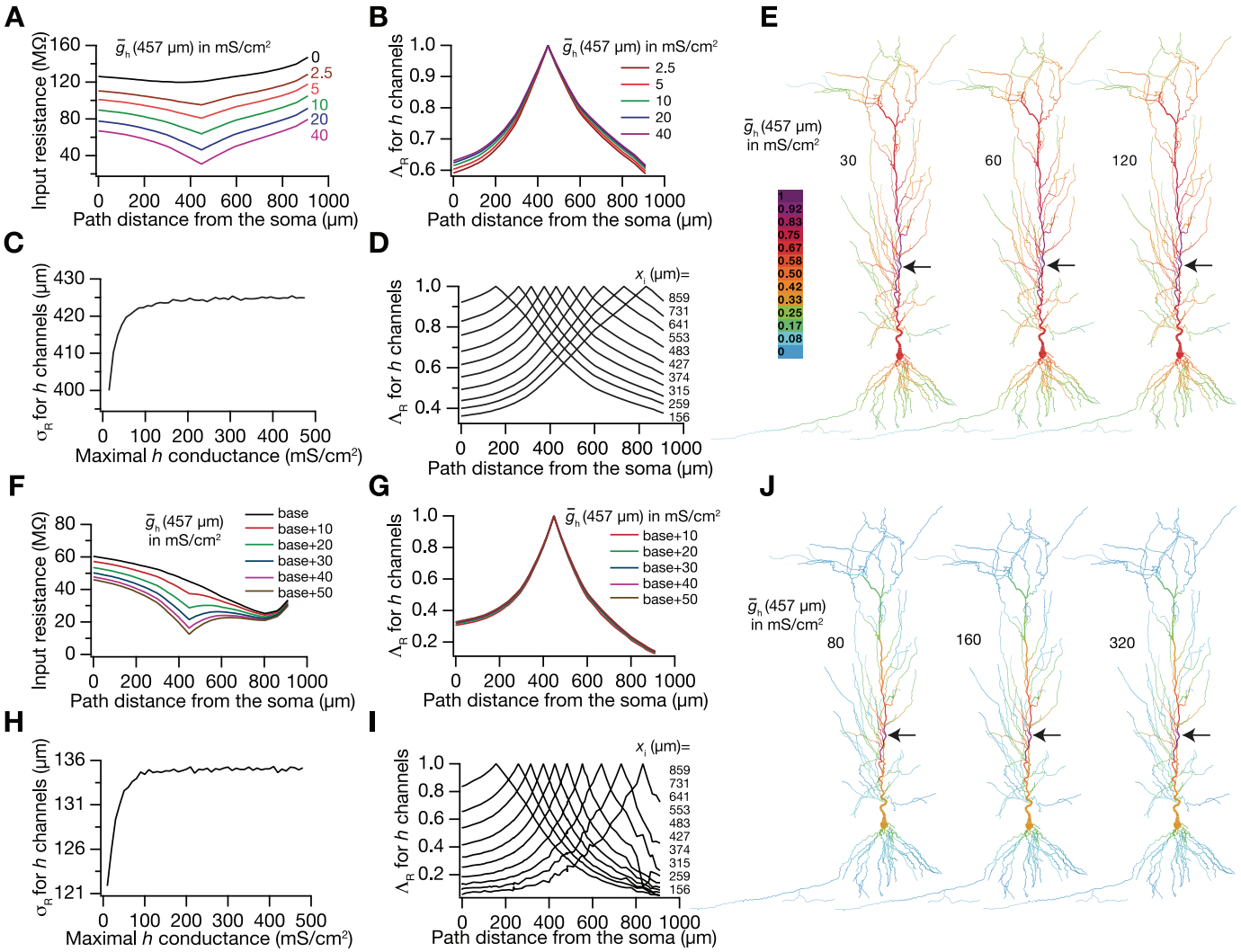

Fig. 3. Local presence of an h-channel cluster exerts widespread influence on R_{in} in a realistic 3-dimensional (3D) model of a CA1 pyramidal neuron and depends on baseline conductance values. *A–E* were derived from simulations performed on a passive model. *A*: R_{in} measured along the somato-apical trunk in the absence (black) and presence of an h-channel cluster, located at 457 μm from the soma and of varying conductance densities ($\bar{g}_h$) (colors). *B*: Λ_R along the somato-apical trunk for various values of $\bar{g}_h$, computed from the plots in *A*. Color codes are the same as those in *A*. *C*: extent of influence σ_R plotted as a function of $\bar{g}_h$. For these simulations, the extent of the influence field was computed as the full width at three-quarter maximum (FWTQM), because the exponential fits never reached a value of 0.5, thus making the computation of full width at half-maximum (FWHM) impossible. *D*: representative plots depicting Λ_R of a single h-channel cluster located at various locations (x_i) on the trunk. *E*: color-coded influence fields across the entire dendritic arbor depicting the influence of a localized h-channel cluster (black arrow; 457 μm from the soma on the trunk) on R_{in}, for various values of $\bar{g}_h$. *F–J*: same as *A–E*, but simulations were performed on a model in which the h conductance values were set to their baseline values (see MODELS AND METHODS). For the sake of comparison with *C*, we computed FWTQM in *H* as well.

tance was higher along the dendritic flank, owing to the higher h-channel density in the terminal dendritic side (*Eq. 4*).

Next we tested the effect of location of h-channel clusters in shaping the extent of influence on R_{in} (cf. Table 1 for the ball-and-stick model). Given that in a multicompartmental model different compartments have different surface areas, we normalized the inserted conductance (specified in mS/cm^2) with respect to surface area of each compartment, such that the inserted conductance (at different locations) was of the same absolute value. In doing so, we found that in the passive 3D model the extent of influence field (σ_R) increased as the distance of cluster from the soma increased (Fig. 3*D*) (σ_R, computed as FWTQM, was closer to 363 μm closer to the soma and increased to ~508 μm closer to the terminal dendrite), whereas in the active 3D model σ_R decreased as the distance between the h-channel cluster and the soma increased (σ_R, computed as FWTQM, was closer to 273 μm closer to the soma and decreased to ~111 μm closer to the terminal dendrite). Again, we attributed these results to the higher density of h channels closer to the terminal dendrite.

Thus far, we have analyzed the influence of VGICs only along the main trunk of the morphologically realistic models. How does the influence of a localized ion channel cluster extend along the entire dendritic tree? To address this, we visualized the influence field across the entire tree with color-coded 2D projections of the entire somatodendritic arbor (using *Eq. 5*) for passive (Fig. 3*E*) and active (Fig. 3*J*) neuronal models. We analyzed the effect of changing the value of the inserted conductance and found that the influence field spanning the entire neuron was not different across various values

of $\bar{g}_h$ in passive (Fig. 3*E*) and active (Fig. 3*J*) neuronal models. Our conclusions that the extent of influence was much lower in the active 3D model through quantitative analysis of the influence field along the trunk (Fig. 3*G*) were further confirmed through comparison of such color-coded 2D projections (Fig. 3*E* vs. Fig. 3*J*). Together, these results suggest that, in a CA1 pyramidal cell, plasticity in distal h-channel densities would have lesser influence than plasticity in proximal locations owing to the baseline gradient in h-channel densities in these neurons.

Finally, we analyzed the influence of an h-channel cluster on another local measurement, f_R, in the passive and active 3D models and found that the properties elucidated with the ball-and-stick model (Table 1) also held in the morphologically realistic models. Furthermore, consistent with previous observations on R_{in}, the extent of influence was much less in the active 3D model compared with the passive 3D model (not shown).

Influence fields for local measurements in thin dendritic branches were confined within the dendritic branch. Given experimental observations about the presence of VGICs and their plasticity in oblique dendrites (Frick et al. 2003; Losonczy and Magee 2006; Losonczy et al. 2008), it was essential to analyze influence fields in obliques and compare them with those in the trunk. Employing R_{in} as the measurement for this analysis, we compared the influence fields of h-channel clusters of the same size present on the main trunk versus on an oblique dendrite in the passive 3D model. As observed above (Fig. 3*E*), the localized presence of an h-channel cluster on the trunk had an influence that spread across a large stretch of the dendritic tree (Fig. 4*A*, *left*). However, when the same cluster was placed on an oblique, its influence field extent was significantly lower compared with that for the cluster on the main trunk, and there was very limited spread of influence beyond the oblique under consideration (Fig. 4*A*, *right*). This reduction in the extent of the influence field in the passive 3D model

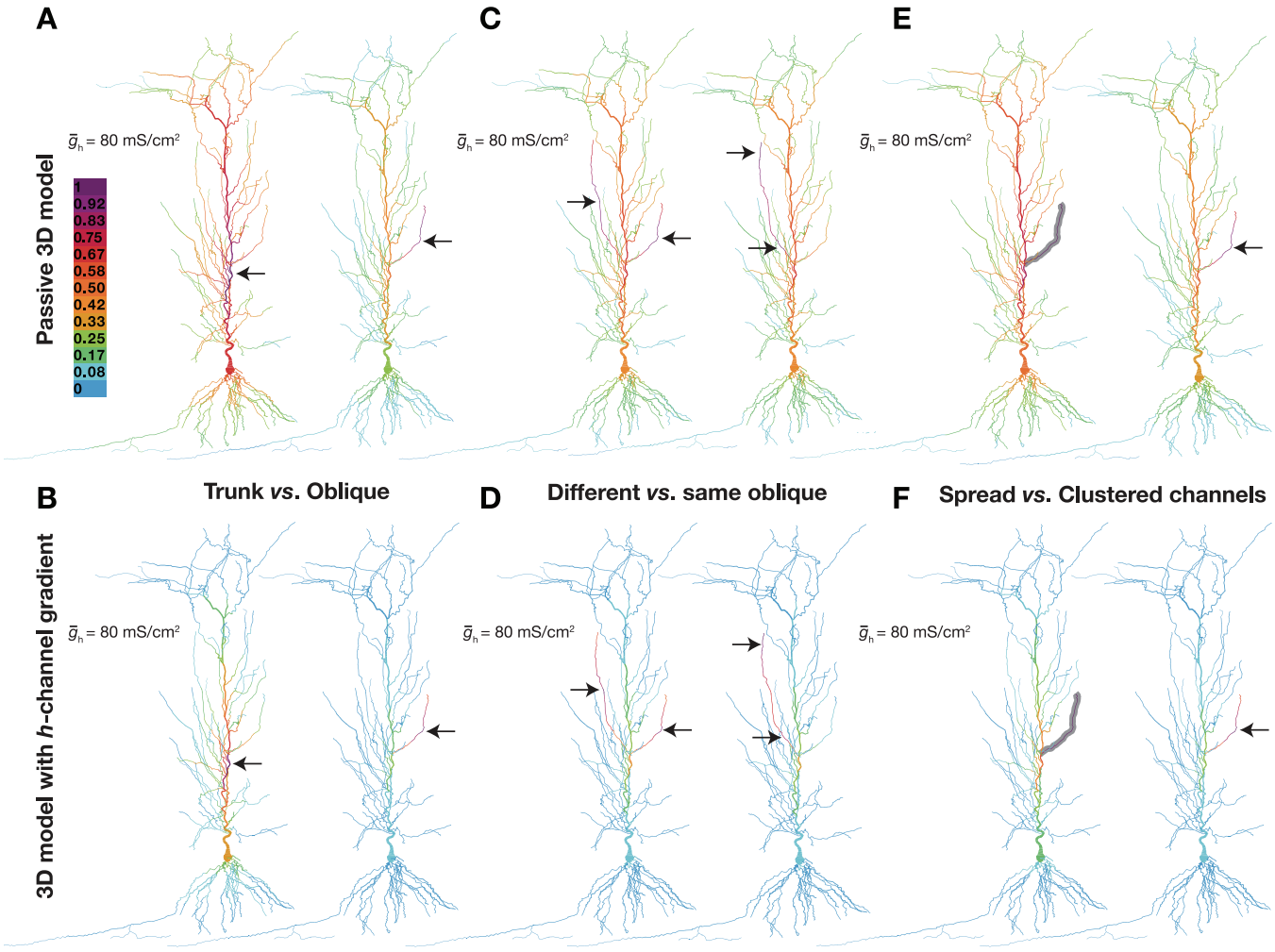

Fig. 4. Influence fields of h-channel clusters and their summation depend on the location of the cluster(s) and baseline conductance distribution in a realistic 3D model of a neuron. *A*, *C*, and *E* were derived from simulations performed on a passive model, whereas *B*, *D*, and *F* were from simulations performed in a model that had a baseline h conductance (active 3D model) (see MODELS AND METHODS). *A* and *B*: color-coded influence field, corresponding to R_{in}, of an h-channel cluster located on the trunk (*left*) vs. an oblique dendrite (*right*), for the passive (*A*) and active (*B*) 3D models. *C* and *D*: color-coded depiction of the summation of influence fields, corresponding to R_{in}, of 2 h-channel clusters present on different (*left*) vs. the same oblique dendritic branch (*right*), for the passive (*C*) and active (*D*) 3D models. In both *C* and *D*, the distance between the 2 clusters is ~250 μm. *E* and *F*: color-coded depiction of the influence field, corresponding to R_{in}, of h channels distributed across the entire oblique branch (*left*) vs. a single cluster of h channels located at the center of the oblique branch (*right*) for the passive (*E*) and active (*F*) 3D models.

could be directly related to the inverse relationship between the diameter of the dendrite and the extent of influence that we had observed with the ball-and-stick model (Table 1). Performing a similar analysis on the active 3D model revealed that the extent of the influence field was much less compared with the passive 3D model (compare Fig. 4*B* with Fig. 4*A*) and, importantly, the influence of an h-channel cluster in an oblique remained confined to the oblique. Thus the reduced diameter of the obliques, coupled with the high background conductance in the active 3D model, ensured that the influences of the presence/plasticity of h-channel clusters in the obliques are confined to that particular oblique.

The contributions of dendritic branches in segregating inputs from various sources and the role of dendritic branches as independent and fundamental computational and plasticity units are well established (Branco and Hausser 2010; Govindarajan et al. 2010; Larkum et al. 2009; London and Hausser 2005; Losonczy and Magee 2006; Losonczy et al. 2008; Nevian et al. 2007; Poirazi et al. 2003; Polsky et al. 2004). For the branches to behave truly as independent subunits, their influence fields (for various measurements) should be limited to the corresponding oblique branches (Fig. 4, *A* and *B*), and the presence of channels in other obliques should not influence measurements in the oblique under consideration. To test whether this was the case, we placed two h-channel clusters in two distinct obliques and asked whether there was overlap in the influence field (Fig. 4*C*). We found that the influences were maximal within the respective obliques, although there was more spread of the influence to the trunk (Fig. 4*C*, *left*), compared with the presence of a single cluster (Fig. 4*A*, *right*). In contrast, when both h-channel clusters were placed on the same oblique, the spread of influence did not significantly stretch into the main trunk (Fig. 4*C*, *right*). We then repeated these experiments in the more realistic active 3D model and asked whether the segregation was more complete in that case. As expected from previous results, the segregation was more complete in the active 3D model (Fig. 4*D*), where the overlap between the influence fields of h-channel clusters on two different obliques was extremely minimal (Fig. 4*D*, *left*). Together, the results so far suggest that the presence and plasticity of h channels in oblique dendrites have spatially confined influence fields with respect to R_{in}, with influences largely limited to the oblique under consideration.

Clustering of ion channels has been demonstrated to modulate physiological properties in multiple systems (Jung and Shuai 2001; Lai and Jan 2006; Shuai and Jung 2003; Vacher et al. 2008). We next asked whether clustering of ion channels introduced significant changes to influence fields compared with the same ion channels distributed evenly across a region. To answer this we chose oblique dendrites, as influence fields in obliques had very limited extents (results above). Specifically, we introduced a single h-channel cluster of a given conductance at the center of the oblique or introduced the same value of h conductance spread across the entire oblique and compared the influence fields in two cases. We found that the influence of the single ion channel cluster was very limited compared with the case in which it was spread across the entire oblique, irrespective of whether we used the passive (Fig. 4*E*) or the active (Fig. 4*F*) 3D model. Similar to previous results, we found that the influence fields have much smaller extents in the active 3D model compared with the passive model.

Influence fields of restorative and regenerative channel clusters for passive propagation properties were spatially widespread. Apart from modulating local properties such as R_{in} and f_R, dendritic VGICs also modulate propagation of electrical signals (Hoffman et al. 1997; Johnston and Narayanan 2008; Magee 2000; Sjostrom et al. 2008; Spruston 2008). How does the presence of VGIC clusters influence propagating properties? Do influence fields corresponding to propagation-related properties taper along both flanks of the cluster location? Are these influence fields affected by the direction of propagation? To answer these questions, we analyzed passive propagation of subthreshold excitatory postsynaptic potentials (EPSPs) and asked how the presence of an A-type K^+- or h-channel cluster affected passive propagation. Similar to our previous analyses, we first established the basic framework, using the ball-and-stick model, and analyzed passive propagation of subthreshold EPSPs with respect to three different conductances: A-type K^+ conductance, h conductance, and persistent Na^+ conductance (see Table 2 for results from the ball-and-stick model) and then analyzed influence fields corresponding to propagating signal in morphologically realistic models.

To analyze the influence of A-type K^+ and h currents on passive propagation of EPSPs in a morphologically realistic model, we inserted an α-current synapse at an apical dendritic compartment 893 μm (path distance) from the soma and an A-type K^+- or h-channel cluster around the center of the apical dendritic shaft (448 μm from the soma) and recorded its amplitude at various locations along the somatodendritic axis (Fig. 5, *B* and *D*). In striking contrast to influence fields corresponding to local properties (Figs. 1–4), we found that the influence was not maximal at the location of the VGIC cluster and did not taper on either side of the cluster location irrespective of the inserted channel type (Fig. 5, *C* and *E*). EPSPs propagate along either side of the synaptic location, and in our case the VGIC cluster was located only along one of these two directions, which we call the cluster direction. We found that the presence of the VGIC cluster did not have any effect on propagation along the no-cluster direction (not shown). For propagation along the cluster direction, the influence was maximal in compartments that were located after the propagating signal crossed the cluster (Fig. 5, *C* and *E*). For compartments between the cluster and the synapse, the influence field was distance dependent, with the influence being maximal at the cluster location. Despite these differences with respect to the influence field properties of local measurements, changing the cluster size by altering the maximal A-type K^+ conductance or h-channel conductance did not significantly alter the influence field properties (Fig. 5, *C* and *E*), thus confirming the invariance of influence fields to cluster size for EPSP propagation as well (Fig. 5, *F* and *G*).

Next, we asked whether the influence of A-type K^+ conductance or h conductance on EPSP propagation was dependent on the location of the cluster. Depending on the cluster direction, we calculated the extent along only one of the two flanks (somatic extent, σ^s_{EPSP} or dendritic extent, σ^d_{EPSP}) and found that the σ^d_{EPSP} increased as a function of the distance between the ion channel cluster and the synaptic location (Fig. 5, *H–J*) irrespective of the ion channel used. Additionally, we also computed σ^s_{EPSP} by placing the synapse proximal to the soma and the ion channel cluster to more distal locations and

Table 2. *Sensitivity analysis for extent of influence fields corresponding to passive propagation of EPSPs and active propagation of action potentials in ball-and-stick model*

Effects of Increase in	Range Tested	Extent of IF of EPSP, σ_{EPSP}			Extent of IF of bAP, σ_{AP}		
		Localized Presence of			Localized Presence of		
		g_h	g_{KA}	g_{NaP}	g_{KA}	g_{Na}	g_M
R_m	1–25 k$\Omega\cdot$cm^2	Increases	Increases	Increases	No effect	No effect	No effect
R_a	20–300 $\Omega\cdot$cm	Decreases	Decreases	Decreases	Decreases	Decreases	Decreases
C_m	0.5–5 μF/cm^2	Decreases	Decreases	Decreases	No effect	No effect	Increases*
Dendritic diameter	0.5–5 μm	Increases	Increases	Increases	Increases	Increases	Increases
$\bar{g}_h$	0–500 mS/cm^2	Increases*					
$\bar{g}_{KA}$	0–500 mS/cm^2		Increases*		No effect		
$\bar{g}_{NaP}$	0–8 mS/cm^2			Decreases*			
$\bar{g}_{Na}$	50–200 mS/cm^2				Decreases	No effect	Decreases
$\bar{g}_M$	0.05–1 S/cm^2						No effect
$\bar{g}_{KDR}$	10–100 mS/cm^2				No effect	No effect	No effect
Activation $V_{1/2}$	−150 to 50 mV	Increases*	Decreases*	Increases*	No effect	Decreases	Decreases
Inactivation $V_{1/2}$	−150 to −20 mV		Decreases*		No effect	No effect	
Distance of cluster from soma	0–500 μm	Depends on location of synapse	Depends on location of synapse	Depends on location of synapse	No effect	No effect	No effect

Sensitivity analysis for the extent of IFs corresponding to passive propagation of excitatory postsynaptic potentials (EPSPs) and active propagation of action potentials in the ball-and-stick model. The parameters on which the analysis was performed form the first column, and the second column indicates the tested range of the corresponding parameter. Other columns correspond to changes observed in σ_{EPSP} and σ_{AP} for increases in the parameters given in the first column corresponding to type of ion channel (top row: *columns 3–8*). *Very small changes. Increase in $V_{1/2}$ refers to depolarizing shift in activation or inactivation $V_{1/2}$ of the A-type K^+ channel.

found that σ^s_{EPSP} decreased as a function of the distance between the ion channel cluster and the synaptic location (not shown). We attributed this to the presence of the large somatic compartment along one flank.

We performed similar analyses in the active 3D model, which had an experimentally constrained baseline gradient of the A-type K^+-channel conductance (see MODELS AND METHODS), and found that the characteristics of the influence fields for EPSP propagation remained similar (not shown). The only difference was that the extent of the influence field was significantly lower in the active 3D model (extent of the influence field varied from 200 to 600 μm, depending on location of the cluster) compared with the passive 3D model (extent of the influence varied from 300 to 750 μm, depending on cluster location; Fig. 5*I*). In summary, in contrast to the influence fields of local properties (Figs. 1–3), the influence of an A-type K^+ channel cluster on passive propagation of EPSPs was not local. The influence field was largely independent of the VGIC conductance, but the direction of propagation, baseline conductance gradients, and the relative location of the ion channel cluster with respect to the synapse were crucial determinants of the influence field in this case.

Influence fields of restorative and regenerative channel clusters for active propagation were spatially confined and location independent. In the analyses above, we found that the influence of localized changes in the A-type K^+ channels on passive propagating properties did not remain local, but had maximal impact on all the compartments located after the propagating signal crossed the cluster (Fig. 5). If this analysis for passive propagation held for backpropagation of action potentials, then it would imply that even localized changes in A-type K^+ channels would cause widespread changes to bAPs, especially at dendritic locations that are beyond the point of plasticity along the propagation direction. However, experimentally, activity-dependent localized changes in the A-channel properties led only to localized changes in the bAP amplitudes (Frick et al. 2004). Even localized application of an A-channel blocker, 4-AP, led only to localized changes in the calcium transients, which reflects only localized changes in bAP amplitude (Frick et al. 2003). We postulated that this difference in spread should be a consequence of the active propagation of bAPs, as opposed to the passive propagation of EPSPs in the cases analyzed before. To test this, we constructed a ball-and-stick model that can sustain active bAPs and studied the influence fields of active propagation with respect to localized changes in A-type K^+ channels, fast Na^+ channels, and slow M-type K^+ channel (Table 2).

After establishing the basic framework for the influence field corresponding to bAP (Λ_{AP}) in the ball-and-stick model using various conductances (Table 2), we analyzed the influence of an A-type K^+-channel cluster on bAP, Λ_{AP}, in two distinct realistic neuronal models (Figs. 6 and 7). One of the models had equal distribution of Na^+ and delayed-rectifier K^+ channels along the somatodendritic compartments, but no other channels in any of the compartments (called the uniform model), and the other had experimentally constrained gradient of A-type K^+ channels in conjunction with Na^+ and delayed-rectifier K^+ channels (called the gradient model) (*Eq. 3*; see MODELS AND METHODS).

We placed an A-type K^+-channel cluster at around the center of the apical trunk and compared the bAP amplitude before and after cluster placement to arrive at Λ_{AP} (Fig. 6*A*). We found that even the localized presence of the cluster affected bAP over a range of compartments in a distance-dependent manner (Fig. 6*B*). However, in contrast to the influence fields corresponding to EPSPs, Λ_{AP} tapered along both the flanks, thus suggesting that the direction of propagation did not play a role in shaping the influence field (Fig. 6*C*). We also found that Λ_{AP} was largely symmetric along the apical trunk (Fig. 6*C*), thus suggesting that the presence of the soma or the direction of propagation did not matter in determining the influence field shapes for active propagation (cf. Fig. 1*D*).

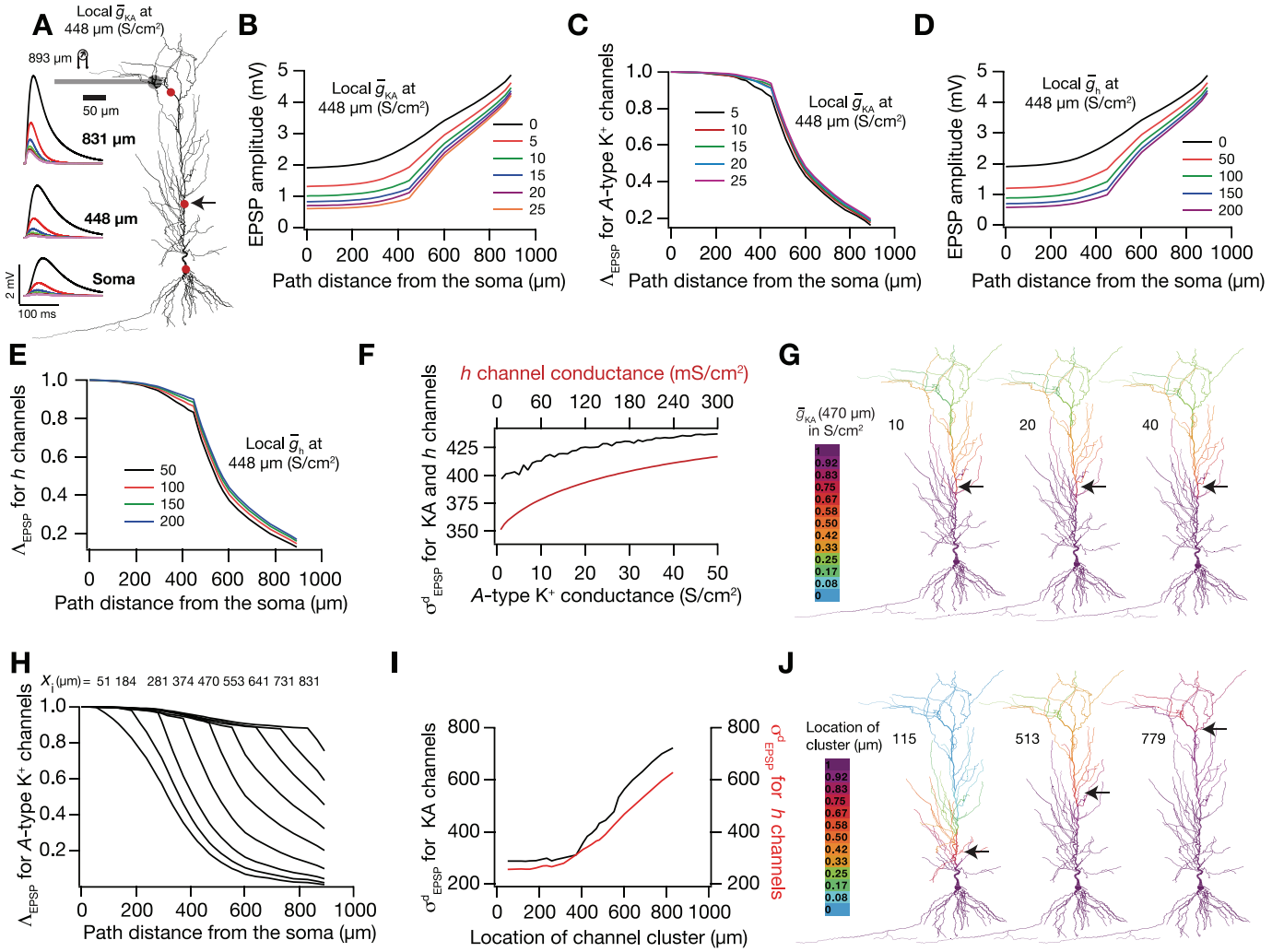

Fig. 5. Influence of local A-type K^+-channel and h-channel clusters on passive propagation in a morphologically realistic 3D model of neuron. *A*: realistic 3D model of neuron showing the location of the α-synapse and recording sites (red dots). An A-type K^+-channel cluster of various conductance ($\bar{g}_{KA}$) values was placed at 448 μm (path distance) from the soma. *B*: plot showing excitatory postsynaptic potential (EPSP) amplitude along the dendrite in the absence (black) and the presence of A-type K^+-channel cluster of various conductance values (colors). *C*: influence field of A-type K^+-channel cluster on EPSP (Λ_{EPSP}) computed from *B* for various values of $\bar{g}_{KA}$. *D* and *E*: similar to *B* and *C*, but EPSP amplitude and Λ_{EPSP} were computed with respect to an h-channel cluster. *F*: plot showing a small and saturating increase in σ^d_{EPSP} for various values of $\bar{g}_{KA}$ (black trace) and values of $\bar{g}_h$ (red trace). *G*: influence field showing the extent of influence of a local A-type K^+-channel cluster of various $\bar{g}_{KA}$, for the entire somatodendritic arbor. *H*: plot showing the Λ_{EPSP} for an A-type K^+ channel cluster placed at various locations (x_i) along the somato-apical trunk. *I*: plot showing the relationship between σ^d_{EPSP} and the location of the cluster with respect to the soma for various values of $\bar{g}_{KA}$ (black trace) and values of $\bar{g}_h$ (red trace). The synapse was fixed at 893 μm from the soma (as depicted in *A*). *J*: color-coded influence field, across the entire somatodendritic arbor, depicting the extent of influence of an A-type K^+-channel cluster present at various locations along the trunk. For all simulations, α-synapse parameters were set as τ = 10 ms, g_{max} = 1.27 nS.

These observations are in agreement with previous experimental findings that activity-dependent localized changes in A-channel properties led only to localized changes in the bAP amplitudes (Frick et al. 2004) and also localized application of the A-channel blocker 4-AP led only to localized changes in the calcium transients, which reflects only localized changes in bAP amplitude (Frick et al. 2003). Finally, the influence field was largely invariant to the cluster size (Fig. 6, *C* and *D*), until a threshold value for $\bar{g}_{KA}$, beyond which the influence field was similar to the passive propagation case. We obtained similar results with the "gradient model," with a difference that the influence field was more asymmetric in the gradient model ($\sigma^d_{AP} > \sigma^s_{AP}$; Fig. 6*G*), owing to the higher baseline $\bar{g}_{KA}$ on the dendritic flank (Fig. 6, *E–H*).

Next, we asked whether Λ_{AP} was dependent on the location of the A-type K^+-channel cluster. Surprisingly, and in contrast with all previous analyzed influence fields, we found that Λ_{AP} was largely invariant to the cluster location (Fig. 7), whenever active propagation was not compromised by the presence of the cluster. This was true for both the uniform model (Fig. 7, *A–C*) and the gradient model (Fig. 7, *D* and *E*), thus confirming the independence of this invariance on baseline A-type K^+-channel densities. When active propagation could not be sustained, Λ_{AP} was similar to Λ_{EPSP} (Fig. 7, *D* and *E*). Together, our results suggest that the influence fields corresponding to active propagation were very different from those for localized properties and for passive propagation. Specifically, Λ_{AP} was spatially confined and was invariant to both the direction of propagation and the size of the cluster.

Influence fields for active propagation in thin dendritic branches were spatially confined within the dendritic branch. We next turned our attention to oblique dendrites in both the

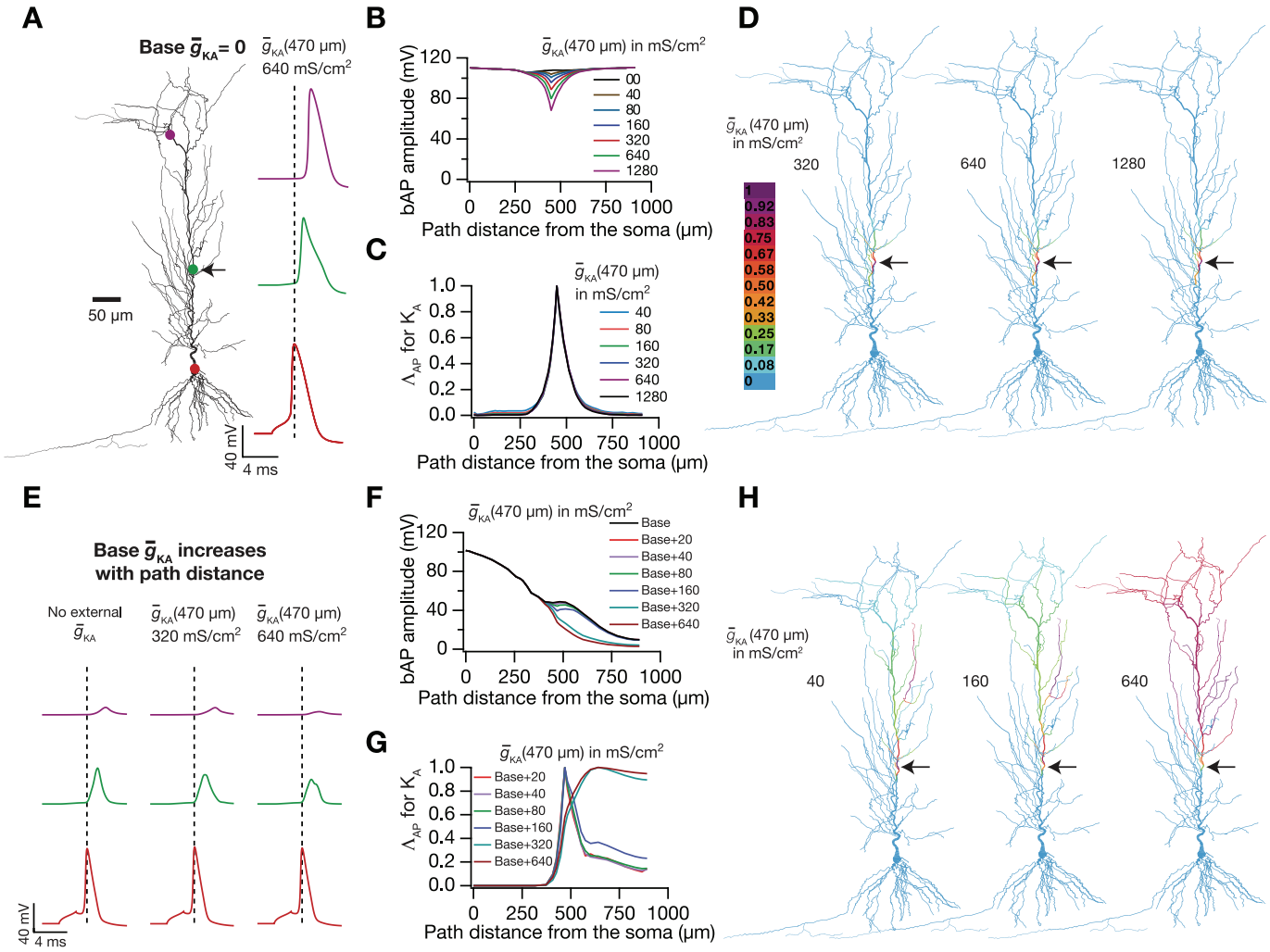

Fig. 6. Local presence of A-type K^+-channel cluster exerts widespread influence on backpropagating action potential (bAP) amplitude in a morphologically realistic 3D model of a neuron. *A–D* were derived from simulations performed on a model with only Na^+ and K_{DR} conductances (uniform 3D model). *A*: reconstructed 3D model of the neuron showing locations where bAP amplitude was measured; red dot at soma, green dot at 470 μm, and purple dot at 880 μm from the soma (path distances). Representative traces depict bAPs recorded at these locations when a cluster of $\bar{g}_{KA}$ (of 640 mS/cm^2) was placed at a distance 470 μm from the soma. *B*: bAP amplitude measured along the somato-apical trunk in the absence (black) and presence of an A-type K^+ channel cluster, located at 470 μm (along the trunk) from the soma and of varying conductance densities ($\bar{g}_{KA}$) (colors). *C*: normalized influence of A-type K^+-channel cluster on bAP amplitude (Λ_{AP}) for various values of $\bar{g}_{KA}$, computed from the plots in *A*. Color codes are the same as those in *A*. *D*: color-coded influence fields across the entire dendritic arbor depicting the influence of a localized A-type K^+ channel cluster (black arrow; 470 μm from the soma on the trunk) on bAP amplitude, for various values of $\bar{g}_{KA}$. *E–H*: same as *A-D*, but simulations were performed on a model that had an additional baseline A-type K^+ conductance gradient (gradient model; see MODELS AND METHODS). This altered the baseline bAP amplitudes as depicted by the black trace in *F*.

uniform and gradient 3D models and analyzed Λ_{AP} in the presence of A-type K^+-channel clusters in these obliques. Our analyses followed the same regime as that we employed for analysis of Λ_R in obliques (Fig. 4). First, we compared the influence fields of A-type K^+-channel clusters of the same size present on the main trunk versus on an oblique dendrite in the uniform (Fig. 8*A*) and gradient (Fig. 8*B*) models. As observed with local properties (Fig. 4, *A* and *B*), with respect to active propagation of bAPs, we found that the influence of an A-type K^+-channel cluster in an oblique remained confined to the oblique (cf. diameter dependence in Table 2). Next, when we placed two different A-type K^+-channel clusters in two distinct obliques, we found that the influences were confined within the respective obliques, irrespective of whether there was one or two clusters in the same oblique (Fig. 8, *A*, *right*, and *C*, *right*) or whether there were two clusters present on two different obliques (Fig. 8*C*, *left*). We observed this confinement of influence fields within obliques, complete with all these invariances, even in the gradient model (Fig. 8*D*). Together, these results suggest that the presence and plasticity of A-type K^+-channel clusters in oblique dendrites have very limited influences on bAP amplitude beyond the oblique. Finally, we asked whether clustering of A-type K^+ channels introduced significant changes to the influence fields compared with the same ion channels distributed evenly across a region. We found that the influence of clustered ion channels was relatively limited compared with the case in which it was spread across the entire oblique, irrespective of whether we used the uniform (Fig. 8*E*) or the gradient (Fig. 8*F*) 3D model. Thus, if the influences of the presence of or plasticity in ion channels were to be confined within the obliques for them to act as independent subunits, clustering of constituent ion channels might offer one solution for implementing this physiologically (cf. Fig. 4).

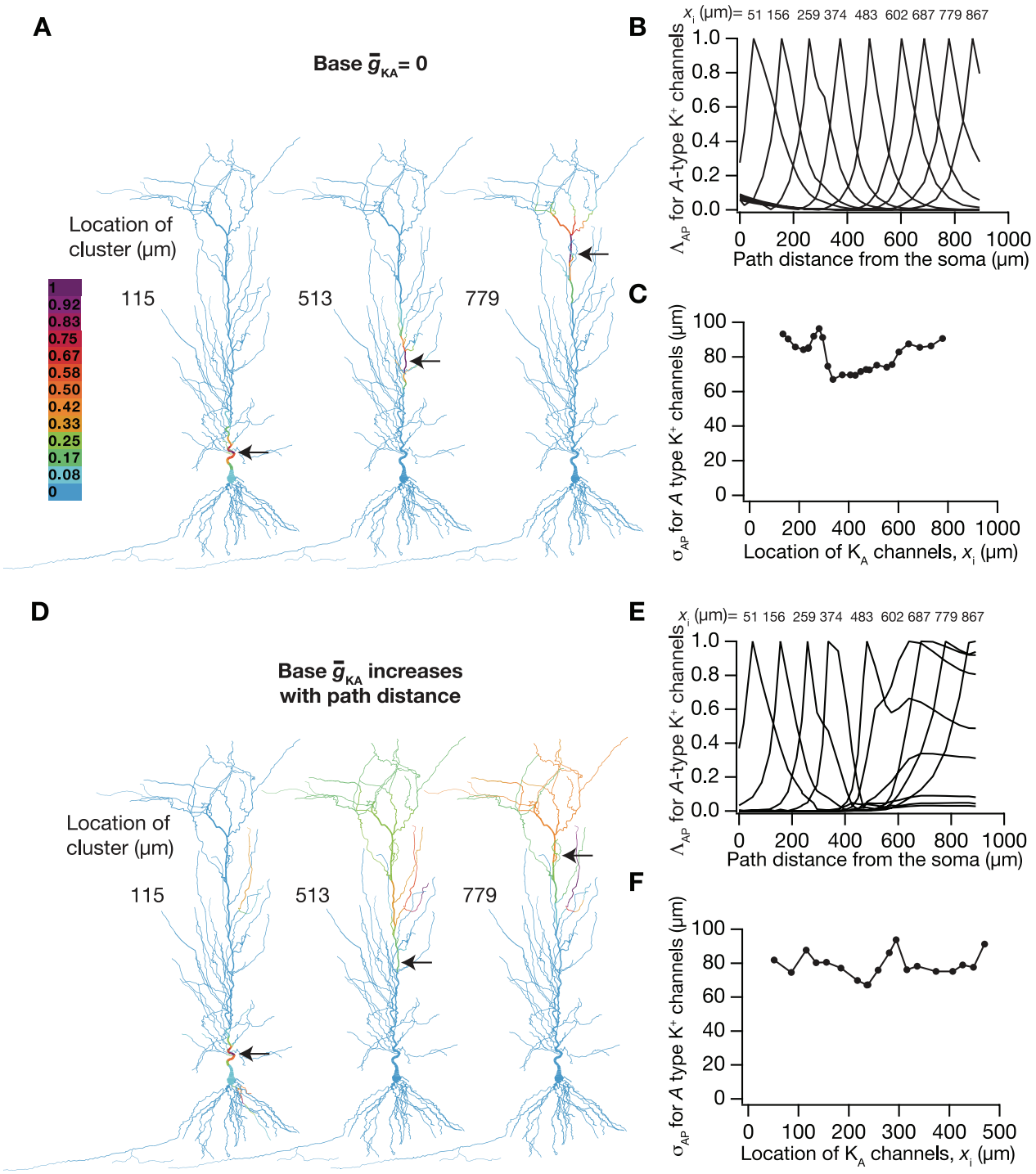

Fig. 7. Extent of influence of A-type K^+-channel cluster is largely independent of the location of A-type K^+-channel cluster on the dendrite in a morphologically realistic 3D neuronal model. *A–C* were derived from simulations performed on a model with only Na^+ and K_{DR} conductances (the uniform 3D model). *A*: color-coded influence fields across the entire dendritic arbor depicting the influence of a localized A-type K^+-channel cluster on bAP amplitude, for various cluster locations (indicated to *left* of each reconstruction). *B*: representative plots depicting influence fields along the somato-apical trunk, corresponding to bAPs, of a single A-type K^+-channel cluster located at various locations (x_i) on the trunk. *C*: extent of influence of a localized A-type K^+-channel cluster on bAP amplitude, σ_{AP}, plotted as function of location of the cluster (x_i) on the dendrite. *D–F*: same as *A–C*, but simulations were performed on the gradient 3D model.

Reconstruction of functional gradients employing influence fields revealed crucial roles for ion channels in adjacent compartments. A primary motivation for the development of the influence fields as a quantitative framework for assessing the roles of dendritic VGICs was its incorporation into learning theory and other neurophysiological models. For this, it would be essential that this abstraction is useful in incorporation of plasticity in ion channels, and importantly in converting such plasticity into functional equivalents, taking into account the influence of such plasticity on physiological measurements in

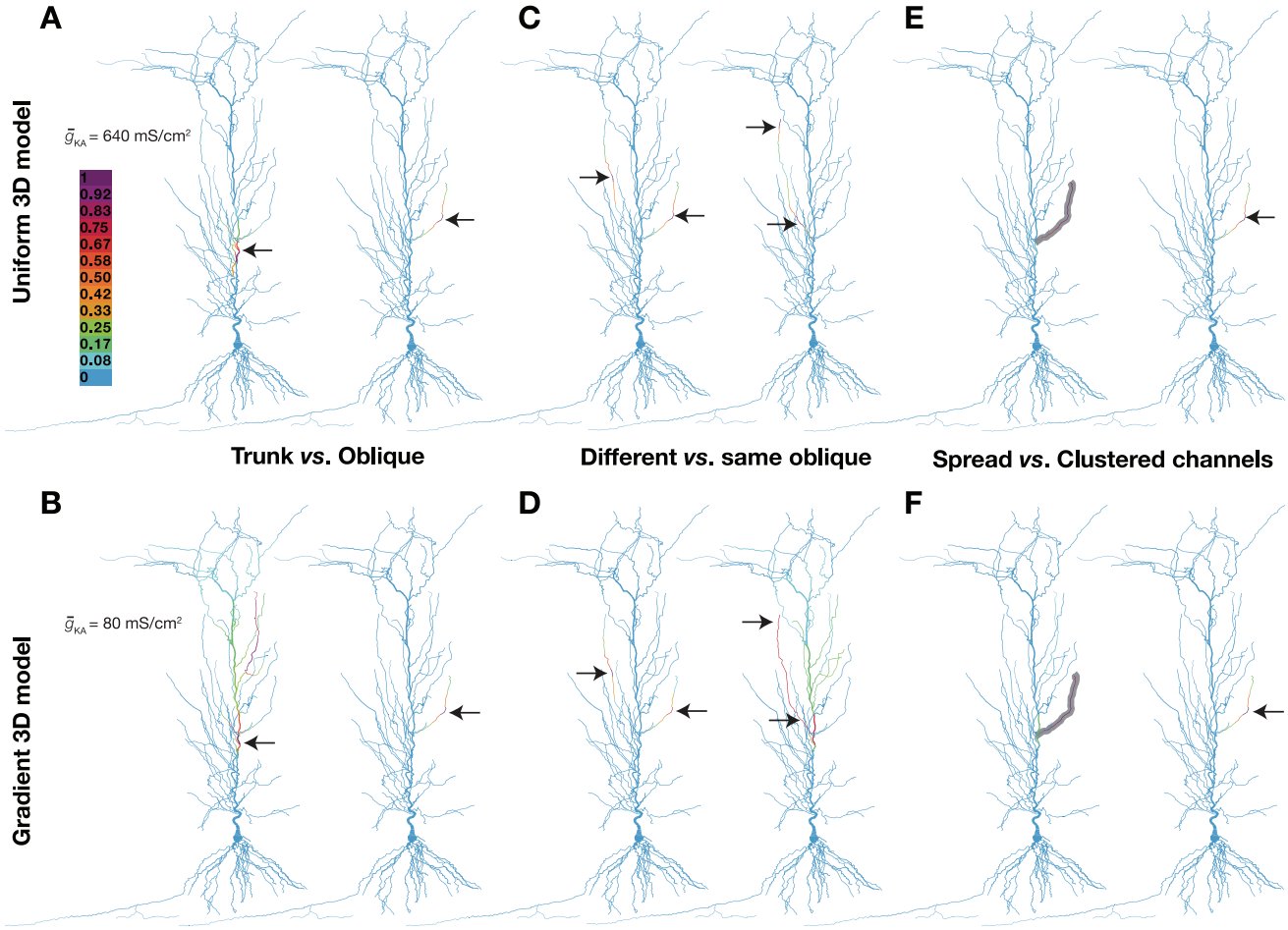

Fig. 8. Location dependence of influence fields of A-type K^+ channel clusters and their summation in a realistic 3D model of a neuron. *A*, *C*, and *E* were derived from simulations performed on a uniform 3D model, whereas *B*, *D*, and *F* were from simulations performed on a gradient 3D model (see MODELS AND METHODS). *A* and *B*: color-coded influence field, corresponding to backpropagation of action potentials, of an A-type K^+-channel cluster located on the trunk (*left*) vs. an oblique dendrite (*right*) for the uniform (*A*) and gradient (*B*) 3D models. *C* and *D*: color-coded depiction of the summation of influence fields, corresponding to backpropagation of action potentials, of 2 A-type K^+-channel clusters present on different (*left*) vs. the same (*right*) oblique dendritic branch, for the uniform (*C*) and gradient (*D*) 3D models. In both *C* and *D*, the distance between the 2 clusters was set at ~250 μm. *E* and *F*: color-coded depiction of the influence field, corresponding to backpropagation of action potentials, of A-type K^+ channels distributed across the entire oblique branch (*left*) vs. a single cluster (of same conductance as the distributed case) of A-type K^+ channels located at the center of the oblique branch (*right*), for the uniform (*E*) and gradient (*F*) 3D models.

other compartments. In short, influence fields should be useful as an abstraction in reconstructing a functional gradient when the distribution and properties of the underlying VGIC are given.

To do this, it was first important to understand how the influence fields of ion channels located at different locations interact with each other. Employing the basic ball-and-stick model, we placed h-channel clusters ($\bar{g}_h$ = 80 mS/cm^2) at two distinct locations on the dendrite and calculated their combined influence field (see MODELS AND METHODS). We found that the summation of influence fields of two h-channel clusters was sublinear with respect to R_{in} (Fig. 9*A*), and the degree of sublinearity increased with increasing distance between the two clusters (Fig. 9*B*). Such increase in sublinearity with increased distance should be expected from our observations related to the location dependence of A_g (Fig. 2) and from the reduction in σ_R with increase in background conductance (Table 1 and Fig. 3). Similar analysis for f_R, using two h-channel clusters, revealed that summation of two $\Lambda_f(x; x_i)$ was sublinear, with the degree of sublinearity decreasing as the distance between two ion channel clusters increased (not shown). Finally, we also found that the dependencies of summation linearity for both R_{in} and f_R were similar when we repeated the analysis with two clusters of M channels, thus confirming that such sublinear summation of the influence fields was channel invariant for these two measurements. However, this sublinearity in summation did not extend to other measurements; when we performed similar analyses with influence fields of A-type K^+ channels on passive and active propagation, we found their summation to be supralinear (Fig. 9, *C* and *D*) and linear (Fig. 9, *E* and *F*), respectively. Thus linearity of summation in the influence fields is critically dependent on the measurement that is being considered.

If the linearity of summation in the influence fields is critically dependent on the measurement, then linearity of summation in the influence fields should be similar even if influence fields were derived from the insertion of two different ion channels (which affect a physiological measurement in a similar fashion) at the two locations. To test this, we placed two different ion channel clusters (A- and M-type K^+-channel clusters) at two different locations along the dendrite and computed linearity of summation of the two different influence

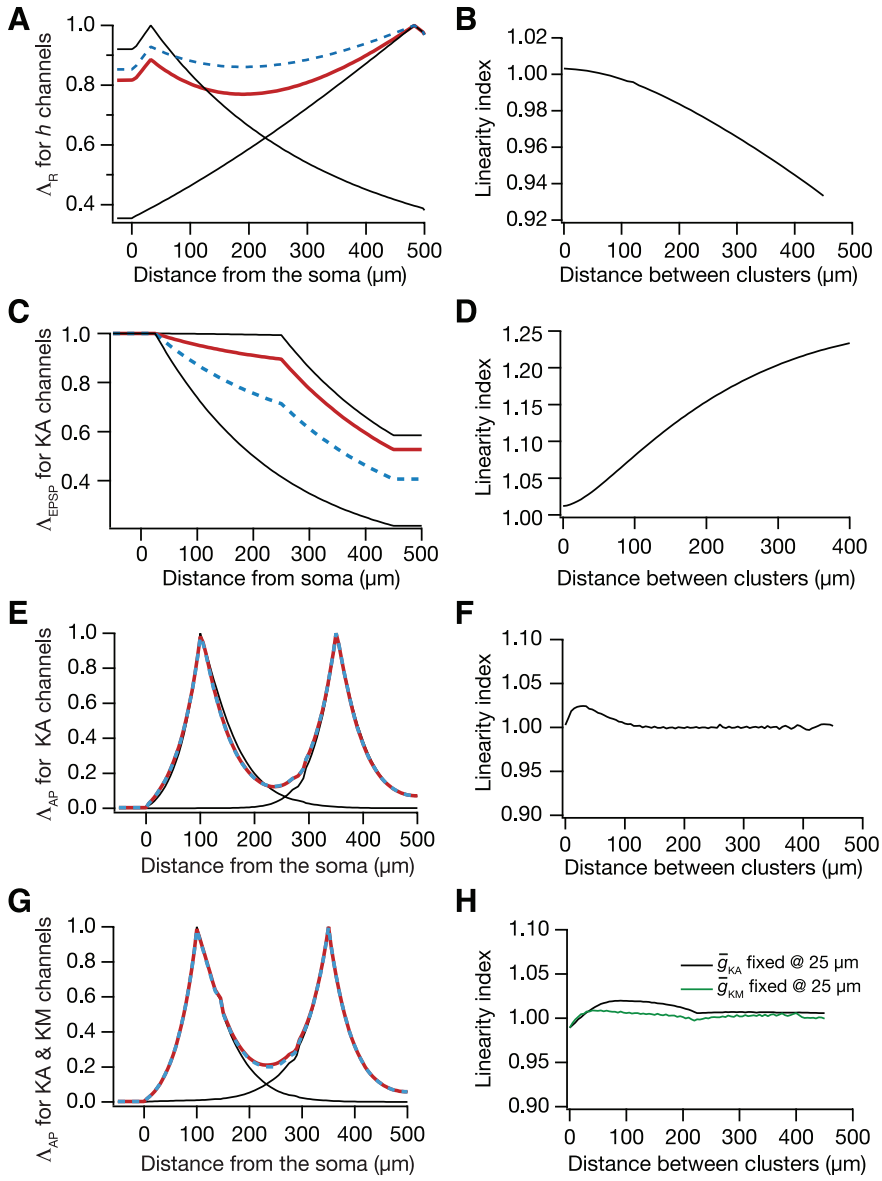

Fig. 9. Linearity of summation in influence fields depends on measurements. *A* and *B*: influence fields of h channels for R_{in} summate sublinearly. *A*: representative plots of Λ_R showing summation of influence fields of 2 h-channel clusters. Black lines represent Λ_R of individual h-channel clusters located at 25 and 475 μm from the soma. Blue dashed line depicts the linear sum of the influence fields of 2 h-channel clusters, whereas red bold line shows the result obtained by placing both clusters simultaneously and measuring Λ_R at various locations. *B*: linearity index (see MODELS AND METHODS) plotted as a function of distance between the 2 h-channel clusters. Analyses were performed by fixing the location of 1 of the 2 clusters (x_i^{fixed} = 25 μm) and varying the other cluster to different locations. *C* and *D*: influence fields of A-type K^+ channels for passive propagation summate supralinearly. *C*: black lines represent Λ_{EPSP} of individual A-type K^+ channel clusters located at 25 and 250 μm from the soma. Color conventions for other plots are similar to *A*. *D*: linearity index plotted as a function of distance between the 2 A-type K^+ channel clusters. x_i^{fixed} = 25 μm, and the synapse was located at 450 μm. *E* and *F*: influence fields of A-type K^+ channels for active propagation summate linearly. *E*: representative plots of Λ_{AP} showing summation of the influence fields of 2 A-type K^+ channel clusters at different locations. Black lines represent Λ_{AP} corresponding to individual A-type K^+ clusters located at 100 and 350 μm from the soma. Color conventions for other plots are similar to *A*. *F*: linearity index plotted as a function of distance between the 2 A-type K^+-channel clusters. x_i^{fixed} = 25 μm. *G* and *H*: influence fields of A-type and M-type K^+ channels for active propagation summate linearly. *G*: representative plots of Λ_{AP} showing summation of the influence fields of A-type K^+-channel cluster located at 100 μm and M-type K^+-channel cluster located at 350 μm from the soma. Black lines represent Λ_{AP} corresponding to individual A-type and M-type K^+ channel clusters located at 100 and 350 μm from the soma, respectively. Color conventions for other plots are similar to *A*. *H*: linearity index plotted as a function of distance between A-type and M-type K^+-channel clusters for 2 cases. Conductances of the A- and M-type K^+ channels were adjusted such that they independently elicited a similar reduction in bAP amplitude when placed at a given location. Black trace: $\bar{g}_{KA}$ fixed at 25 μm and location of $\bar{g}_M$ varied; green trace: $\bar{g}_M$ fixed at 25 μm and location of $\bar{g}_{KA}$ varied.

fields (Fig. 9*G*). We found that the linearity index for summation between these two clusters was close to unity, irrespective of the distance between the two clusters (Fig. 9, *G* and *H*). However, when we analyzed such cross-channel interaction across measurements with different combinations of restorative and regenerative conductances, we found that linearity of summation was dependent on whether the channels were of the same type (restorative vs. regenerative) and the locations and the magnitudes of the cluster. Such dependencies would be critical in understanding the interactions between different somatic and dendritic channels and their roles in regulating neuronal physiology (George et al. 2009; Pavlov et al. 2011), and influence fields provide a quantitative framework for understanding such cross-channel interactions.

To enable simplicity of reconstruction of the functional gradient, we chose the A-type K^+ channel and active propagation, given the linearity in the summations of its influence fields (Fig. 9, *E* and *F*). To accomplish the demonstration that the proposed abstraction is capable of such reconstruction, we introduced a known A-type K^+-channel density gradient into the ball-and-stick model. The distance-dependent gradient in the maximal A-type K^+-channel density was represented as $\bar{g}_{KA}(x)$, where x represented distance from the soma. $\bar{g}_{KA}(x)$ was set as follows (Fig. 10*B*), in order to obtain a bAP amplitude of ~10 mV at the terminal dendritic location of the model (500 μm from the soma):

$$\bar{g}_{KA}(x) = 57\left(1 + 5\frac{x}{100}\right)\text{mS/cm}^2 \qquad (16)$$

With this gradient in A-type K^+ channels assigned, we measured the bAP amplitude at various locations along the somatodendritic axis and called that the actual measurement [$bAP^{actual}(x)$, with x being the distance from the soma].

Now, we wanted to test whether we could approximate this actual measurement by just knowing the properties of the channel, its relationship to the measurement, and the channel's influence field with respect to that measurement. Influence fields were represented with their two-exponential characterization (*Eq. 7*), taking into account the location dependence of

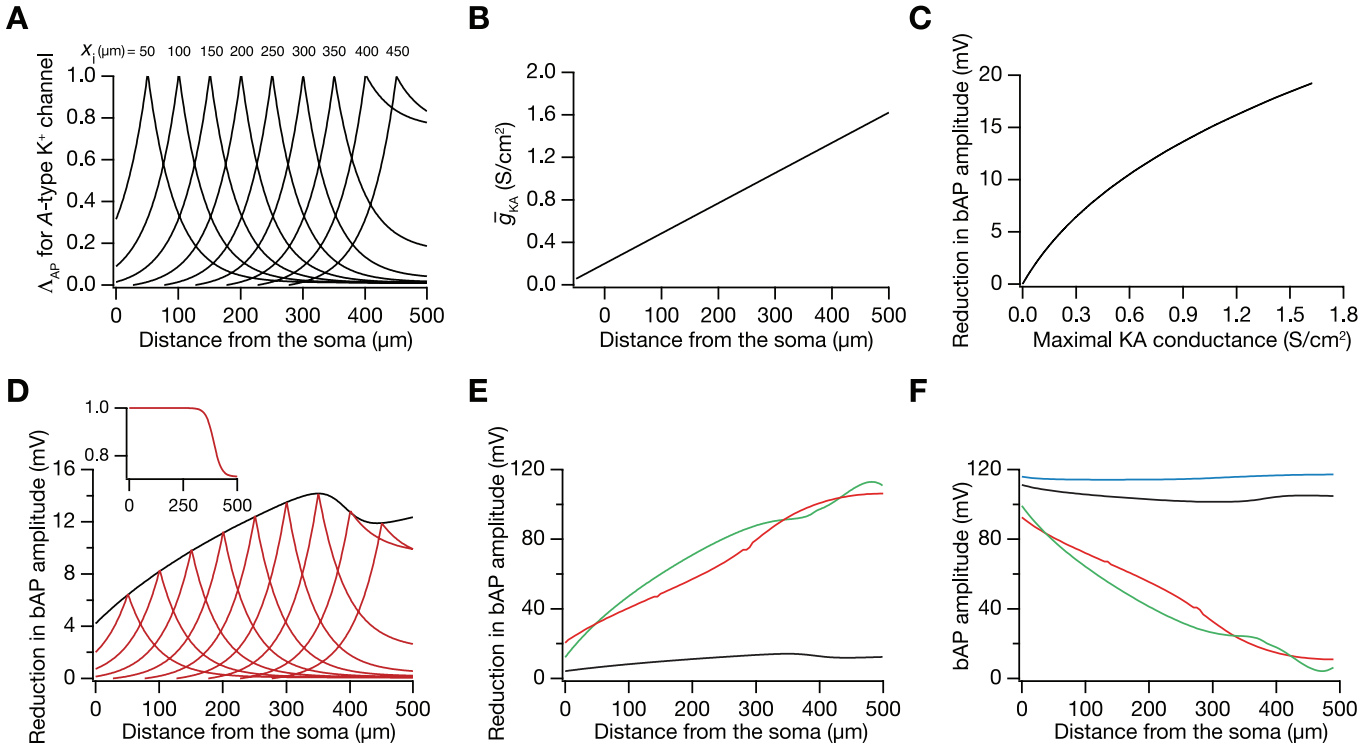

Fig. 10. Reconstruction of functional gradients using influence fields. *A*: Λ_{AP} reconstructed using its functional form. It may be noted that the shape of the influence field is dependent on the location of the ion channel cluster, x_i, by comparing the Λ_{AP} for $x_i = 100$ μm and for $x_i = 400$ μm. *B*: somatodendritic gradient in maximal A-type K^+ conductance, $\bar{g}_{KA}$, introduced into the piston model. *C*: empirically determined reduction in bAP amplitude plotted as a function of $\bar{g}_{KA}$, without taking location of ion channel cluster, x_i, into account. A channel cluster with various $\bar{g}_{KA}$ was inserted at the center of the dendritic compartment (250 μm from the soma), and the reduction in bAP amplitude at that location was computed for each value of $\bar{g}_{KA}$. *D*, *inset*: normalized dependence of amount of reduction in bAP amplitude as a function of x_i. Black line: estimate of reduction in bAP amplitude without taking influence fields into account. This was obtained from *B*, *C*, and *inset* in *D*. Red lines: representative influence fields (shown in *A*) multiplied by values shown in black traces, in a location-dependent manner. *E*: comparison of estimates of reductions in bAP amplitudes obtained after taking (green) and not taking (black; same as black in *D*) influence fields into account with the actual reductions in bAP amplitudes (red). *F*: comparison of estimates obtained after taking (green) and not taking (black) influence fields into account with the actual reductions in bAP amplitudes (red). Green and black plots were obtained by subtracting correspondingly color-coded plots in *E* from the bAP values obtained in the absence of any A-type K^+ channel in the model (shown in cyan).

Λ_{AP}, especially along the dendritic flank. Through this abstraction, we obtained a continuous functional representation of $\Lambda_{AP}(x; x_i)$ for all x and x_i (Fig. 10*A*).

The influence field is a relative measurement that quantifies the spread of influence along the neuronal topograph. To reconstruct the functional gradient from the channel gradient, we need to know the relationship, at the location of the VGIC conductance, between the functional measurement under consideration (bAP amplitude) and the conductance magnitude of the VGIC (A-type K^+ channel). We empirically found that the local reduction in bAP amplitude as a function of the cluster size ($\bar{g}_{KA}$), $\Delta bAP_{local}(\bar{g}_{KA})$, to be as in Fig. 10*C*, and the local reduction was maximal when the cluster was closer to the soma (Fig. 10*D*, *inset*).

We first considered the case in which there was no influence of VGIC conductances in adjacent compartments on physiological measurements in a given compartment. This would imply that the amount of reduction in bAP amplitude would just be a direct transformation from $\bar{g}_{KA}$ as a function of distance (*Eq. 16*; Fig. 10*B*) to reductions in local bAP amplitude, using the transformation shown in Fig. 10*C*. We represented this direct transformation of local $\bar{g}_{KA}$ to reduction in bAP amplitude as $\Delta bAP_{noIF}(\bar{g}_{KA},x_i)$, and found that $\Delta bAP_{noIF}(\bar{g}_{KA},x_i)$ (Fig. 10, *D* and *E*) was much smaller than the actual reductions obtained with simulations (Fig. 10*E*). This quantitatively demonstrated that the amount of reduction in bAP amplitude at a given location was not just dependent on the A-type K^+ channels at that location.

Next, in order to account for influences of all other clusters, we first calculated the local bAP reduction $\Delta bAP_{noIF}(\bar{g}_{KA},x_i)$ for each cluster location x_i. We then calculated the influence fields $\Lambda_{AP}(x; x_i)$ as in Fig. 10*A* and multiplied this with $\Delta bAP_{noIF}(\bar{g}_{KA},x_i)$ of the corresponding cluster location x_i. This single-product term $[\Lambda_{AP}(x; x_i)\cdot\Delta bAP_{noIF}(\bar{g}_{KA},x_i)]$ varies with location x and provides us with the amount of reduction in bAP amplitude at each location x owing to the presence of a single A-type K^+ channel cluster located at x_i with conductance $\bar{g}_{KA}(x_i)$ (Fig. 10*D*). Now, to account for influences of all A-type K^+ channel clusters on the bAP amplitude at a given location x, we just computed the sum of all such product values (each corresponding to a different cluster location x_i) at that particular location x:

$$\Delta bAP_{IF}(x) = \int_0^{L_d} \Delta bAP_{noIF}(\bar{g}_{KA}, x_i)\Lambda_{AP}(x; x_i)dx_i \quad (17)$$

Performing this computation for all x provided us with an estimate of the reduction of bAP amplitude as a function of distance (Fig. 10*E*) due to the presence of a $\bar{g}_{KA}(x)$ as in *Eq. 16*. We compared this estimated change in bAP (Fig. 10*E*) with the

actual change in bAP we obtained from $bAP^{actual}(x)$ (Fig. 10*E*) and found that this estimate was much closer to the actual bAP changes. If influences from adjacent compartments were absent, the maximal reduction in bAP amplitude was just ~14 mV maximum (Fig. 10*D*) with $\bar{g}_{KA}(x)$ distributed as in *Eq. 16*. In reality, the maximal reduction in bAP amplitude was ~100 mV, which can be obtained only when the distance-dependent influence of other ion channel clusters is accounted for (Fig. 10, *E* and *F*). Thus a large proportion of bAP reduction (~86 mV in this case) is through influences from adjacent VGICs, with the channel cluster at that location contributing only a minor component. Finally, it must be noted that this reconstruction process (as in *Eq. 17*) yields close approximations to the measurement only because influence fields of bAPs summate linearly (Fig. 9, *E* and *F*). If, on the other hand, the influence fields summate sublinearly (as in R_{in}; Fig. 9, *A* and *B*) or supralinearly (as in EPSPs; Fig. 9, *C* and *D*), then *Eq. 17* needs modifications to account for this sub-/supralinearity of summation.

Together, the "influence field" framework provides a quantitative means for converting ion channel properties to different intrinsic properties (not just gain/excitability) at various locations, thus making it feasible to relate local/global plasticity in specific VGIC properties to location-dependent changes in any of these physiological properties. This provides a quantitative framework to incorporate rules for plasticity in VGICs, and study the role of various intrinsic properties within learning theory frameworks, in the same way as plasticity in synaptic weights has been studied within learning theory and other neurophysiological frameworks (Dayan and Abbott 2001; Haykin 1998).

DISCUSSION

The prime goal of this study was to develop a quantitative framework for analyzing dendritic VGICs, accounting for the connected nature of neuronal compartments and the consequent nonlocal influences of VGIC conductances. We developed a quantitative abstraction of such influences, and called it the "influence field" of that VGIC conductance. Analyses involving multiple ion channels and different local as well as propagating physiological properties presented a multitude of conclusions that are critical to the understanding of single neurons and their information processing capabilities. A prominent conclusion that is critical for models of single-neuron computation is that a given VGIC conductance can have distinct influences on different physiological measurements. The structure, the spatial extent, and the location dependence of influence fields, their summation with respect to different clusters of the same VGIC type, and sensitivities to various parameters are all heavily dependent on the specific measurement under consideration (Tables 1 and 2). However, we also found some important influence field characteristics that were invariant across measurements. First, influence fields were largely independent on the VGIC conductance magnitude. Second, the influence of ion channels located in obliques was spatially confined to those obliques alone. This offers an excellent segregation mechanism in terms of VGIC location and plasticity, thus enabling oblique dendrites to act as independent and fundamental physiological and computational subunits (Branco and Hausser 2010; Govindarajan et al. 2010; Larkum et al. 2009; Losonczy and Magee 2006; Losonczy et al. 2008; Polsky et al. 2004).

Influence fields in metaplasticity and homeostasis. The presence of VGICs in dendrites entails their role in processing subthreshold (Branco et al. 2010; Branco and Hausser 2011; Hutcheon and Yarom 2000; Llinas 1988; London and Hausser 2005; Magee 2000; O'Donnell and Nolan 2011; Sjostrom et al. 2008; Spruston 2008; Stemmler and Koch 1999) as well as suprathreshold (Bean 2007; Christie and Westbrook 2003; Hoffman et al. 1997; Kim et al. 2005; Losonczy et al. 2008) electrical signals. Hence, presence of or plasticity in VGICs could modulate rules governing the induction of synaptic plasticity (Fan et al. 2005; Frick et al. 2004; Johnston et al. 2003; Lin et al. 2008; Lujan et al. 2009; Narayanan and Johnston 2010; Shah et al. 2010; Watanabe et al. 2002). Given our results that even localized plasticity in VGICs can alter physiological properties in a large stretch of a neuron, plasticity in VGICs would alter synaptic plasticity rules at locations away from the location of VGIC plasticity. However, as influence fields of VGICs in thin dendritic branches remain largely confined to that branch alone (Figs. 3*B* and 7*B*), plasticity in VGICs in a given dendritic branch would lead to modulation of synaptic plasticity rules only within that branch, thus leading to branch-specific metaplasticity.

Small perturbations in the balance between excitation and inhibition can modulate the input-output relationship of a neuron and lead to changes in network dynamics and neural coding (Atallah and Scanziani 2009; Chagnac-Amitai and Connors 1989; Kirkwood and Bear 1994; Kriegstein 1987; Nelson 1991; Pouille et al. 2009; Turrigiano 2011; Turrigiano and Nelson 2004). In neurons like the CA1 pyramidal cell, inputs to the neuron from different brain regions are spatially segregated along the topograph of the neuron. In neurons like these, if a perturbation in the balance between excitation and inhibition occurs through inputs from one brain region, it would be easy if this perturbation were handled through local changes without significantly affecting other regions. Given that active membrane conductances have been shown to adapt themselves in order to maintain the input-output relationship of a neuron and to adapt with changing network dynamics (Aizenman et al. 2003; Brager and Johnston 2007; Brickley et al. 2001; Desai 2003; Desai et al. 1999a, 1999b; Fan et al. 2005; Golowasch et al. 1999; Narayanan and Johnston 2007; van Welie et al. 2004, 2006), we propose that localized plasticity in VGICs can provide one solution to this problem. As influence fields of VGICs spread across the neuronal topograph, such plasticity could be directed in such a way that it affects inputs only onto one specific subregion of the neuron, thus establishing global homeostasis through localized changes in specific ion channel densities (cf. efficient coding hypothesis below).

Influence fields and learning theory. A prime motivation in the development of the quantitative framework presented here was the development of a learning theory framework that would include dendritic VGICs and their plasticity, apart from synaptic plasticity. One postulate that has gained attention in the literature is that the diverse ion channels and the diverse forms of plasticity in VGICs could be playing a role in enabling neurons to efficiently encode incoming network information. Under this framework, neurons, by adapting their intrinsic properties through alterations in VGICs and other intrinsic mechanisms, could match their response properties to

those of network statistics to efficiently encode information. Against this background, during learning (or pathological states), incoming network information is altered, and the process of changing synaptic and intrinsic properties in an effort to match them with this altered network statistics would constitute the cellular basis for learning and associated homeostasis [cf. efficient coding hypothesis in the systems framework (Barlow 1961; Geisler 2008; Simoncelli 2003; Simoncelli and Olshausen 2001)]. As different dendritic subregions of a neuron could receive inputs from different brain regions, there would be a necessity for different regions to adapt to different network statistics. In such a case, in the process of learning incoming statistics, and matching intrinsic responses differentially at various somatodendritic locations, different regions would have different VGIC distributions (Lundstrom et al. 2008; Narayanan and Johnston 2007, 2008b; Nelson and Turrigiano 2008; O'Donnell and Nolan 2011; Stemmler and Koch 1999).

If learning models are to be developed to test the efficient coding hypothesis in single-neuron computation, it would be required to find *1*) what response properties different VGICs encode; *2*) how (synaptic and intrinsic plasticity) learning rules and network statistics relate to changes in neuronal response properties; and *3*) how the presence and plasticity of a localized VGIC influence different properties at different locations along the neuron. In this context, the nonlocal influences of VGICs form an important distinction between intrinsic plasticity and synaptic plasticity, and could be a mechanism in bringing about global order through local computations. Specifically, influence fields of different measurements could play roles analogous to those of interneuronal Mexican hat-like coupling in the self-organized development of sensory maps (Goodhill 2007; Swindale 1996). Influence fields constitute abstracted quantifications of interactions between compartments within a single neuron, as opposed to the Mexican hat interactions between neurons, but could play a similar role in translating local plasticity to global order spanning the entire neuron.

From the above discussion, it is also obvious that focusing on gain/excitability as the only property that VGICs modulate would not constitute an overarching framework for their incorporation into learning frameworks (Johnston and Narayanan 2008; Llinas 1988; Marder et al. 1996; Narayanan and Johnston 2008a; O'Donnell and Nolan 2011; Remme et al. 2010; Wang 2010). It would be important to recognize that ion channels modulate various measurements, and could be enabling the neuron in modulating its response properties to specific features of the incoming input (Losonczy et al. 2008; Narayanan and Johnston 2007; O'Donnell and Nolan 2011). Incorporating these into learning frameworks, apart from providing a quantitative framework for understanding neuronal learning, would also help in developing efficient algorithms for learning and classifying patterns. Thus far, such efforts have been limited to abstractions of synaptic plasticity (Haykin 1998), which could be made more efficient by incorporating physiological measurements that active dendrites and their plasticity alter, and thus efficiently harnessing the enormous computational power of a single neuron. Such efforts would also help in answering questions on what specific roles the nonlocal and differential influence fields play, on whether they enforce some interactions between synapses located in adjacent compartments and help in a global mutually dependent homeostatic self-organization of various physiological properties within a neuron (Andrasfalvy et al. 2008; Chen et al. 2010; Nelson and Turrigiano 2008; O'Donnell and Nolan 2011; Rabinowitch and Segev 2006; Shin and Chetkovich 2007).

Interactions between cross-channel influence fields. In this study, we employed simplified neuronal models with a restricted range of ion channels to develop a basic framework for how VGICs influence a cross section of measurements in adjacent neuronal compartments, and how such influence fields interact with each other (Fig. 9). When more types of dendritic VGICs are present, as in a more realistic neuronal model, the interactions between the various restorative and regenerative conductances present in different compartments in an elaborate dendritic tree would become more complex. Extensions to this basic framework could thus focus on elucidating the complexities associated with interactions between multiple types of ion channels present in different dendritic compartments.

In this context, a growing body of experimental literature has focused on the analysis of colocalization of multiple types of channels, whereby their combined presence endows a compartment with very distinct "emergent" physiological properties (Anderson et al. 2010; George et al. 2009; Park et al. 2010; Pavlov et al. 2011; Tsay et al. 2007; Wang et al. 2010). In such cases, it stands to reason that the distance between clusters of these different ion channel types would play a crucial role in how they alter the observed phenomenon. For instance, if one channel type (say, a calcium channel) were localized in the dendrites and the other (say, a calcium-dependent K^+ channel) in the soma, the influence of one on the other would be dependent on the distance between them and various passive and active properties. The framework presented here provides an ideal setup for analyzing such influences, through effective quantification of such cross-channel interactions. The basic framework presented here could also be extended to analyze other physiological phenomena, which are not necessarily electrical in nature. For instance, the framework could easily be extended to encompass reaction-diffusion mechanisms for analyzing the microdomains associated with biochemical signaling entities located at specific neuronal compartments (Kennedy et al. 2005; Kotaleski and Blackwell 2010) and their influence on plasticity (or other phenomenon) in physiological properties of other compartments. Finally, from our analysis, we note that an increase in any background conductance always led to a reduction in the extent of the influence field. Thus influence fields in in vivo conditions would be much less compared with in vitro conditions because of the high-conductance state in vivo (Chance et al. 2002).

Experimental determination of influence fields. How can we measure influence fields experimentally? A direct way to do this would be the use of the dynamic clamp procedure to inject a point conductance at a neuronal location and record the measurement of interest from various locations along the neuron (Sharp et al. 1993; Williams 2004). Using a similar experimental paradigm, Williams (2004) tested conductance compartmentalization in cortical pyramidal neurons. Although the author used generalized conductance changes, and measured voltage changes to steady-state current pulses to arrive at the conclusion on spatial compartmentalization of conductances (Williams 2004), the results are in general agreement with the shape of the influence field for various measurements and their independence of the magnitude of the respective

conductances. However, as different measurements are differentially dependent on various ion channels (Tables 1 and 2), it would be necessary to test influence fields for each of such measurement-ion channel pairs through the injection of appropriate conductances. Coupling such experiments with appropriate pharmacological agents could also help in understanding the dependencies of various physiological measurements on a given influence field.

Another way to measure influence fields would be to use either calcium or voltage imaging techniques so that measurements might be acquired over the entire topograph of the neuron rather than being restricted to a single location (as above). This technique has been used effectively in assessing the influence of A-type K^+ current on bAPs. With calcium imaging, it has been demonstrated that changes in calcium transients are localized in response to a localized reduction in A current, achieved either through activity-dependent changes (Frick et al. 2004) or through pharmacologically induced localized blockade (Frick et al. 2003). Although indirect, it may be noted that the shape of extent of influence of such changes is consistent with our results (Fig. 7). Finally, if extracellular correlates to specific measurements could be found, microelectronic methods that are being developed for extending extracellular measurements into the three-dimensional domain (Du et al. 2009; Wise et al. 2008) could be useful in obtaining the influence of a localized ion channel cluster on various parts of a neuron.

In summary, in this study we formulated a generalized quantitative framework of influence fields for analyzing functional gradients within single neurons and picked certain propagating and localized properties to assess their influence fields with respect to specific VGICs. We presented methods by which such a framework could help in including dendritic ion channels and their plasticity in learning theory within a broad framework of efficient encoding of neuronal information, thus harnessing the full computational potential of single neurons. Future studies could focus on developing theoretical and experimental frameworks employing influence fields as abstractions for active dendrites and their plasticity, and on experimentally measuring influence fields for various measurements.

ACKNOWLEDGMENTS

The authors thank Dr. Daniel Johnston for helpful comments on a draft of this manuscript.

GRANTS

A career development award to R. Narayanan from the International Human Frontier Science Program Organization and the Indian Institute of Science supported this study.

DISCLOSURES

No conflicts of interest, financial or otherwise, are declared by the author(s).

AUTHOR CONTRIBUTIONS

Author contributions: R.K.R. and R.N. conception and design of research; R.K.R. and R.N. performed experiments; R.K.R. and R.N. analyzed data; R.K.R. and R.N. interpreted results of experiments; R.K.R. and R.N. prepared figures; R.K.R. and R.N. drafted manuscript; R.K.R. and R.N. edited and revised manuscript; R.K.R. and R.N. approved final version of manuscript.

REFERENCES

Aizenman CD, Akerman CJ, Jensen KR, Cline HT. Visually driven regulation of intrinsic neuronal excitability improves stimulus detection in vivo. *Neuron* 39: 831–842, 2003.

Anderson D, Mehaffey WH, Iftinca M, Rehak R, Engbers JD, Hameed S, Zamponi GW, Turner RW. Regulation of neuronal activity by Cav3-Kv4 channel signaling complexes. *Nat Neurosci* 13: 333–337, 2010.

Andrasfalvy BK, Makara JK, Johnston D, Magee JC. Altered synaptic and non-synaptic properties of CA1 pyramidal neurons in Kv4.2 KO mice. *J Physiol* 586: 3881–3892, 2008.

Ascoli GA, Donohue DE, Halavi M. NeuroMorpho.Org: a central resource for neuronal morphologies. *J Neurosci* 27: 9247–9251, 2007.

Atallah BV, Scanziani M. Instantaneous modulation of gamma oscillation frequency by balancing excitation with inhibition. *Neuron* 62: 566–577, 2009.

Barlow HB. Possible principles underlying the transformation of sensory messages. In: *Sensory Communication*, edited by Rosenblith WA. Cambridge, MA: MIT Press, 1961, p. 217–234.

Bean BP. The action potential in mammalian central neurons. *Nat Rev Neurosci* 8: 451–465, 2007.

Bernard C, Anderson A, Becker A, Poolos NP, Beck H, Johnston D. Acquired dendritic channelopathy in temporal lobe epilepsy. *Science* 305: 532–535, 2004.

Brager DH, Johnston D. Plasticity of intrinsic excitability during long-term depression is mediated through mGluR-dependent changes in I_h in hippocampal CA1 pyramidal neurons. *J Neurosci* 27: 13926–13937, 2007.

Branco T, Clark BA, Hausser M. Dendritic discrimination of temporal input sequences in cortical neurons. *Science* 329: 1671–1675, 2010.

Branco T, Hausser M. Synaptic integration gradients in single cortical pyramidal cell dendrites. *Neuron* 69: 885–892, 2011.

Branco T, Hausser M. The single dendritic branch as a fundamental functional unit in the nervous system. *Curr Opin Neurobiol* 20: 494–502, 2010.

Brickley SG, Revilla V, Cull-Candy SG, Wisden W, Farrant M. Adaptive regulation of neuronal excitability by a voltage-independent potassium conductance. *Nature* 409: 88–92, 2001.

Carnevale NT, Hines ML. *The NEURON Book*. Cambridge, UK: Cambridge Univ. Press, 2006.

Chagnac-Amitai Y, Connors BW. Horizontal spread of synchronized activity in neocortex and its control by GABA-mediated inhibition. *J Neurophysiol* 61: 747–758, 1989.

Chance FS, Abbott LF, Reyes AD. Gain modulation from background synaptic input. *Neuron* 35: 773–782, 2002.

Chen X, Johnston D. Properties of single voltage-dependent K^+ channels in dendrites of CA1 pyramidal neurones of rat hippocampus. *J Physiol* 559: 187–203, 2004.

Chen X, Shu S, Schwartz LC, Sun C, Kapur J, Bayliss DA. Homeostatic regulation of synaptic excitability: tonic $GABA_A$ receptor currents replace I_h in cortical pyramidal neurons of HCN1 knock-out mice. *J Neurosci* 30: 2611–2622, 2010.

Christie JM, Westbrook GL. Regulation of backpropagating action potentials in mitral cell lateral dendrites by A-type potassium currents. *J Neurophysiol* 89: 2466–2472, 2003.

Colbert CM, Magee JC, Hoffman DA, Johnston D. Slow recovery from inactivation of Na^+ channels underlies the activity-dependent attenuation of dendritic action potentials in hippocampal CA1 pyramidal neurons. *J Neurosci* 17: 6512–6521, 1997.

Dayan P, Abbott LF. *Theoretical Neuroscience: Computational and Mathematical Modeling of Neural Systems*. Cambridge, MA: MIT Press, 2001.

Desai NS. Homeostatic plasticity in the CNS: synaptic and intrinsic forms. *J Physiol (Paris)* 97: 391–402, 2003.

Desai NS, Rutherford LC, Turrigiano GG. BDNF regulates the intrinsic excitability of cortical neurons. *Learn Mem* 6: 284–291, 1999a.

Desai NS, Rutherford LC, Turrigiano GG. Plasticity in the intrinsic excitability of cortical pyramidal neurons. *Nat Neurosci* 2: 515–520, 1999b.

Du J, Riedel-Kruse IH, Nawroth JC, Roukes ML, Laurent G, Masmanidis SC. High-resolution three-dimensional extracellular recording of neuronal activity with microfabricated electrode arrays. *J Neurophysiol* 101: 1671–1678, 2009.

Fan Y, Fricker D, Brager DH, Chen X, Lu HC, Chitwood RA, Johnston D. Activity-dependent decrease of excitability in rat hippocampal neurons through increases in I_h. *Nat Neurosci* 8: 1542–1551, 2005.

Fleidervish IA, Lasser-Ross N, Gutnick MJ, Ross WN. Na^+ imaging reveals little difference in action potential-evoked Na^+ influx between axon and soma. *Nat Neurosci* 13: 852–860, 2010.

Frick A, Magee J, Johnston D. LTP is accompanied by an enhanced local excitability of pyramidal neuron dendrites. *Nat Neurosci* 7: 126–135, 2004.

Frick A, Magee J, Koester HJ, Migliore M, Johnston D. Normalization of Ca^{2+} signals by small oblique dendrites of CA1 pyramidal neurons. *J Neurosci* 23: 3243–3250, 2003.

Geisler WS. Visual perception and the statistical properties of natural scenes. *Annu Rev Psychol* 59: 167–192, 2008.

George MS, Abbott LF, Siegelbaum SA. HCN hyperpolarization-activated cation channels inhibit EPSPs by interactions with M-type K^+ channels. *Nat Neurosci* 12: 577–584, 2009.

Golowasch J, Abbott LF, Marder E. Activity-dependent regulation of potassium currents in an identified neuron of the stomatogastric ganglion of the crab *Cancer borealis*. *J Neurosci* 19: RC33, 1999.

Goodhill GJ. Contributions of theoretical modeling to the understanding of neural map development. *Neuron* 56: 301–311, 2007.

Govindarajan A, Israely I, Huang SY, Tonegawa S. The dendritic branch is the preferred integrative unit for protein synthesis-dependent LTP. *Neuron* 69: 132–146, 2010.

Haykin S. *Neural Networks: A Comprehensive Foundation*. Upper Saddle River, NJ: Prentice Hall, 1998.

Hoffman DA, Magee JC, Colbert CM, Johnston D. K^+ channel regulation of signal propagation in dendrites of hippocampal pyramidal neurons. *Nature* 387: 869–875, 1997.

Hu H, Vervaeke K, Storm JF. Two forms of electrical resonance at theta frequencies, generated by M-current, h-current and persistent Na^+ current in rat hippocampal pyramidal cells. *J Physiol* 545: 783–805, 2002.

Hutcheon B, Yarom Y. Resonance, oscillation and the intrinsic frequency preferences of neurons. *Trends Neurosci* 23: 216–222, 2000.

Johnston D, Christie BR, Frick A, Gray R, Hoffman DA, Schexnayder LK, Watanabe S, Yuan LL. Active dendrites, potassium channels and synaptic plasticity. *Philos Trans R Soc Lond B Biol Sci* 358: 667–674, 2003.

Johnston D, Narayanan R. Active dendrites: colorful wings of the mysterious butterflies. *Trends Neurosci* 31: 309–316, 2008.

Jung P, Shuai JW. Optimal sizes of ion channel clusters. *Europhys Lett* 56: 29–35, 2001.

Kennedy MB, Beale HC, Carlisle HJ, Washburn LR. Integration of biochemical signalling in spines. *Nat Rev Neurosci* 6: 423–434, 2005.

Kim J, Wei DS, Hoffman DA. Kv4 potassium channel subunits control action potential repolarization and frequency-dependent broadening in rat hippocampal CA1 pyramidal neurones. *J Physiol* 569: 41–57, 2005.

Kim SJ, Linden DJ. Ubiquitous plasticity and memory storage. *Neuron* 56: 582–592, 2007.

Kirkwood A, Bear MF. Hebbian synapses in visual cortex. *J Neurosci* 14: 1634–1645, 1994.

Kotaleski JH, Blackwell KT. Modelling the molecular mechanisms of synaptic plasticity using systems biology approaches. *Nat Rev Neurosci* 11: 239–251, 2010.

Kriegstein AR. Synaptic responses of cortical pyramidal neurons to light stimulation in the isolated turtle visual system. *J Neurosci* 7: 2488–2492, 1987.

Lai HC, Jan LY. The distribution and targeting of neuronal voltage-gated ion channels. *Nat Rev Neurosci* 7: 548–562, 2006.

Larkum ME, Nevian T, Sandler M, Polsky A, Schiller J. Synaptic integration in tuft dendrites of layer 5 pyramidal neurons: a new unifying principle. *Science* 325: 756–760, 2009.

Legenstein R, Maass W. Branch-specific plasticity enables self-organization of nonlinear computation in single neurons. *J Neurosci* 31: 10787–10802, 2011.

Lin MT, Lujan R, Watanabe M, Adelman JP, Maylie J. SK2 channel plasticity contributes to LTP at Schaffer collateral-CA1 synapses. *Nat Neurosci* 11: 170–177, 2008.

Llinas RR. The intrinsic electrophysiological properties of mammalian neurons: insights into central nervous system function. *Science* 242: 1654–1664, 1988.

London M, Hausser M. Dendritic computation. *Annu Rev Neurosci* 28: 503–532, 2005.

Losonczy A, Magee JC. Integrative properties of radial oblique dendrites in hippocampal CA1 pyramidal neurons. *Neuron* 50: 291–307, 2006.

Losonczy A, Makara JK, Magee JC. Compartmentalized dendritic plasticity and input feature storage in neurons. *Nature* 452: 436–441, 2008.

Lujan R, Maylie J, Adelman JP. New sites of action for GIRK and SK channels. *Nat Rev Neurosci* 10: 475–480, 2009.

Lundstrom BN, Higgs MH, Spain WJ, Fairhall AL. Fractional differentiation by neocortical pyramidal neurons. *Nat Neurosci* 11: 1335–1342, 2008.

Magee JC. Dendritic hyperpolarization-activated currents modify the integrative properties of hippocampal CA1 pyramidal neurons. *J Neurosci* 18: 7613–7624, 1998.

Magee JC. Dendritic integration of excitatory synaptic input. *Nat Rev Neurosci* 1: 181–190, 2000.

Marder E, Abbott LF, Turrigiano GG, Liu Z, Golowasch J. Memory from the dynamics of intrinsic membrane currents. *Proc Natl Acad Sci USA* 93: 13481–13486, 1996.

Martin SJ, Grimwood PD, Morris RG. Synaptic plasticity and memory: an evaluation of the hypothesis. *Annu Rev Neurosci* 23: 649–711, 2000.

Migliore M, Hoffman DA, Magee JC, Johnston D. Role of an A-type K^+ conductance in the back-propagation of action potentials in the dendrites of hippocampal pyramidal neurons. *J Comput Neurosci* 7: 5–15, 1999.

Migliore M, Shepherd GM. Emerging rules for the distributions of active dendritic conductances. *Nat Rev Neurosci* 3: 362–370, 2002.

Mozzachiodi R, Byrne JH. More than synaptic plasticity: role of nonsynaptic plasticity in learning and memory. *Trends Neurosci* 33: 17–26, 2010.

Narayanan R, Dougherty KJ, Johnston D. Calcium store depletion induces persistent perisomatic increases in the functional density of h channels in hippocampal pyramidal neurons. *Neuron* 68: 921–935, 2010.

Narayanan R, Johnston D. Long-term potentiation in rat hippocampal neurons is accompanied by spatially widespread changes in intrinsic oscillatory dynamics and excitability. *Neuron* 56: 1061–1075, 2007.

Narayanan R, Johnston D. The ascent of channels with memory. *Neuron* 60: 735–738, 2008a.

Narayanan R, Johnston D. The h channel mediates location dependence and plasticity of intrinsic phase response in rat hippocampal neurons. *J Neurosci* 28: 5846–5860, 2008b.

Narayanan R, Johnston D. The h current is a candidate mechanism for regulating the sliding modification threshold in a BCM-like synaptic learning rule. *J Neurophysiol* 104: 1020–1033, 2010.

Nelson SB. Temporal interactions in the cat visual system. III. Pharmacological studies of cortical suppression suggest a presynaptic mechanism. *J Neurosci* 11: 369–380, 1991.

Nelson SB, Turrigiano GG. Strength through diversity. *Neuron* 60: 477–482, 2008.

Neves G, Cooke SF, Bliss TV. Synaptic plasticity, memory and the hippocampus: a neural network approach to causality. *Nat Rev Neurosci* 9: 65–75, 2008.

Nevian T, Larkum ME, Polsky A, Schiller J. Properties of basal dendrites of layer 5 pyramidal neurons: a direct patch-clamp recording study. *Nat Neurosci* 10: 206–214, 2007.

O'Donnell C, Nolan MF. Tuning of synaptic responses: an organizing principle for optimization of neural circuits. *Trends Neurosci* 34: 51–60, 2011.

Park CY, Shcheglovitov A, Dolmetsch R. The CRAC channel activator STIM1 binds and inhibits L-type voltage-gated calcium channels. *Science* 330: 101–105, 2010.

Pavlov I, Scimemi A, Savtchenko L, Kullmann DM, Walker MC. I_h-mediated depolarization enhances the temporal precision of neuronal integration. *Nat Commun* 2: 199, 2011.

Poirazi P, Brannon T, Mel BW. Pyramidal neuron as two-layer neural network. *Neuron* 37: 989–999, 2003.

Polsky A, Mel BW, Schiller J. Computational subunits in thin dendrites of pyramidal cells. *Nat Neurosci* 7: 621–627, 2004.

Poolos NP, Migliore M, Johnston D. Pharmacological upregulation of h-channels reduces the excitability of pyramidal neuron dendrites. *Nat Neurosci* 5: 767–774, 2002.

Pouille F, Marin-Burgin A, Adesnik H, Atallah BV, Scanziani M. Input normalization by global feedforward inhibition expands cortical dynamic range. *Nat Neurosci* 12: 1577–1585, 2009.

Pyapali GK, Sik A, Penttonen M, Buzsaki G, Turner DA. Dendritic properties of hippocampal CA1 pyramidal neurons in the rat: intracellular staining in vivo and in vitro. *J Comp Neurol* 391: 335–352, 1998.

Rabinowitch I, Segev I. The endurance and selectivity of spatial patterns of long-term potentiation/depression in dendrites under homeostatic synaptic plasticity. *J Neurosci* 26: 13474–13484, 2006.

Remme MW, Lengyel M, Gutkin BS. Democracy-independence trade-off in oscillating dendrites and its implications for grid cells. *Neuron* 66: 429–437, 2010.

Remy S, Beck H, Yaari Y. Plasticity of voltage-gated ion channels in pyramidal cell dendrites. *Curr Opin Neurobiol* 20: 503–509, 2010.

Shah MM, Anderson AE, Leung V, Lin X, Johnston D. Seizure-induced plasticity of h channels in entorhinal cortical layer III pyramidal neurons. *Neuron* 44: 495–508, 2004.

Shah MM, Hammond RS, Hoffman DA. Dendritic ion channel trafficking and plasticity. *Trends Neurosci* 33: 307–316, 2010.

Shah MM, Migliore M, Valencia I, Cooper EC, Brown DA. Functional significance of axonal Kv7 channels in hippocampal pyramidal neurons. *Proc Natl Acad Sci USA* 105: 7869–7874, 2008.

Sharp AA, O'Neil MB, Abbott LF, Marder E. Dynamic clamp: computer-generated conductances in real neurons. *J Neurophysiol* 69: 992–995, 1993.

Shin M, Chetkovich DM. Activity-dependent regulation of h channel distribution in hippocampal CA1 pyramidal neurons. *J Biol Chem* 282: 33168–33180, 2007.

Shuai JW, Jung P. Optimal ion channel clustering for intracellular calcium signaling. *Proc Natl Acad Sci USA* 100: 506–510, 2003.

Simoncelli EP. Vision and the statistics of the visual environment. *Curr Opin Neurobiol* 13: 144–149, 2003.

Simoncelli EP, Olshausen BA. Natural image statistics and neural representation. *Annu Rev Neurosci* 24: 1193–1216, 2001.

Sjostrom PJ, Rancz EA, Roth A, Hausser M. Dendritic excitability and synaptic plasticity. *Physiol Rev* 88: 769–840, 2008.

Spruston N. Pyramidal neurons: dendritic structure and synaptic integration. *Nat Rev Neurosci* 9: 206–221, 2008.

Stemmler M, Koch C. How voltage-dependent conductances can adapt to maximize the information encoded by neuronal firing rate. *Nat Neurosci* 2: 521–527, 1999.

Stevens CF. A million dollar question: does LTP = memory? *Neuron* 20: 1–2, 1998.

Swindale NV. The development of topography in the visual cortex: a review of models. *Network* 7: 161–247, 1996.

Triesch J. Synergies between intrinsic and synaptic plasticity mechanisms. *Neural Comput* 19: 885–909, 2007.

Tsay D, Dudman JT, Siegelbaum SA. HCN1 channels constrain synaptically evoked Ca^{2+} spikes in distal dendrites of CA1 pyramidal neurons. *Neuron* 56: 1076–1089, 2007.

Turrigiano G. Too many cooks? Intrinsic and synaptic homeostatic mechanisms in cortical circuit refinement. *Annu Rev Neurosci* 34: 89–103, 2011.

Turrigiano GG, Nelson SB. Homeostatic plasticity in the developing nervous system. *Nat Rev Neurosci* 5: 97–107, 2004.

Uebachs M, Opitz T, Royeck M, Dickhof G, Horstmann MT, Isom LL, Beck H. Efficacy loss of the anticonvulsant carbamazepine in mice lacking sodium channel beta subunits via paradoxical effects on persistent sodium currents. *J Neurosci* 30: 8489–8501, 2010.

Vacher H, Mohapatra DP, Trimmer JS. Localization and targeting of voltage-dependent ion channels in mammalian central neurons. *Physiol Rev* 88: 1407–1447, 2008.

van Welie I, van Hooft JA, Wadman WJ. Background activity regulates excitability of rat hippocampal CA1 pyramidal neurons by adaptation of a K^+ conductance. *J Neurophysiol* 95: 2007–2012, 2006.

van Welie I, van Hooft JA, Wadman WJ. Homeostatic scaling of neuronal excitability by synaptic modulation of somatic hyperpolarization-activated Ih channels. *Proc Natl Acad Sci USA* 101: 5123–5128, 2004.

Vervaeke K, Hu H, Graham LJ, Storm JF. Contrasting effects of the persistent Na^+ current on neuronal excitability and spike timing. *Neuron* 49: 257–270, 2006.

Wang XJ. Neurophysiological and computational principles of cortical rhythms in cognition. *Physiol Rev* 90: 1195–1268, 2010.

Wang Y, Deng X, Mancarella S, Hendron E, Eguchi S, Soboloff J, Tang XD, Gill DL. The calcium store sensor, STIM1, reciprocally controls Orai and CaV1.2 channels. *Science* 330: 105–109, 2010.

Wang Z, Xu NL, Wu CP, Duan S, Poo MM. Bidirectional changes in spatial dendritic integration accompanying long-term synaptic modifications. *Neuron* 37: 463–472, 2003.

Watanabe S, Hoffman DA, Migliore M, Johnston D. Dendritic K^+ channels contribute to spike-timing dependent long-term potentiation in hippocampal pyramidal neurons. *Proc Natl Acad Sci USA* 99: 8366–8371, 2002.

Weber C, Triesch J. A sparse generative model of V1 simple cells with intrinsic plasticity. *Neural Comput* 20: 1261–1284, 2008.

Williams SR. Spatial compartmentalization and functional impact of conductance in pyramidal neurons. *Nat Neurosci* 7: 961–967, 2004.

Wise KD, Sodagar AM, Yao Y, Gulari MN, Perlin GE, Najafi K. Microelectrodes, microelectronics and implantable neural microsystems. *Proc IEEE*: 1184–1202, 2008.

Zhang W, Linden DJ. The other side of the engram: experience-driven changes in neuronal intrinsic excitability. *Nat Rev Neurosci* 4: 885–900, 2003.